THE PUBLIC ADVOCATES OFFICE
CALIFORNIA PUBLIC UTILITIES COMMISSION

Order Instituting Investigation on the Commission's Own Motion into the Operations and Practices of Southern California Gas Company with Respect to the Aliso Canyon storage facility and the release of natural gas, and Order to Show Cause Why Southern California Gas Company Should Not Be Sanctioned for Allowing the Uncontrolled Release of Natural Gas from Its Aliso Canyon Storage Facility

**SUPPORTING ATTACHMENTS
OF
MINA BOTROS
MATTHEW TAUL
ALAN BACH
TYLER HOLZSCHUH**

San Francisco, California
June 30, 2020

i

Supporting Attachments

Page[1]	Document
591	SoCalGas' Response to SED-DR-060, q. 7(c)
593	Blade's response to SED-DR-058, q. 1.2
599	www.glossary.oilfield.slb.com/en/Terms/c/ casing-inspection_log.aspx Schlumberger's Definition of Casing Inspection Log
601	www.slb.com/-/media/files/production/product-sheet/usi Schlumberger's Product Description of USIT
604	www.glossary.oilfield.slb.com/en/Terms/f/flux_leakage.aspx Schlumberger's Definition of Flux Leakage
606	A. J. Hayman, R. Hutin, and P. V. Wright, *High-Resolution Cementation and Corrosion Imaging By Ultrasound* (1991)
632	sphweb.bumc.bu.edu/otlt/MPH-Modules/BS/BS704_ Confidence_Intervals/BS704_Confidence_Intervals_print.html "Confidence Intervals," Lisa Sullivan, PhD.

---

[1] In the Public Advocates Office Opening Testimony, the Supporting Attachments were numbered from CalAdvocates - 001 to CalAdvocates - 590. In the Public Advocates Office Sur-Reply Testimony, the page numbering begins at CalAdvocates - 591.

SoCalGas' Response to SED-DR-060, q. 7(c)

ORDER INSTITUTING INVESTIGATION ON THE COMMISSION'S OWN MOTION INTO THE OPERATIONS AND PRACTICES OF SOUTHERN CALIFORNIA GAS COMPANY WITH RESPECT TO THE ALISO CANYON STORAGE FACILITY AND THE RELEASE OF NATURAL GAS, AND ORDER TO SHOW CAUSE WHY SOUTHERN CALIFORNIA GAS COMPANY SHOULD NOT BE SANCTIONED FOR ALLOWING THE UNCONTROLLED RELEASE OF NATURAL GAS FROM ITS ALISO CANYON STORAGE FACILITY (I.19-06-016)

SOUTHERN CALIFORNIA GAS COMPANY

(DATA REQUEST SED-SCG-60 DATED MARCH 31, 2020)

SOCALGAS RESPONSE DATED APRIL 13, 2020

1991 paper by Atlas Wireline Services reported that Multichannel Vertilog was a newly developed version of the Vertilog flux leakage tool called Digital Vertilog (see SoCalGas Reply Testimony, Chapter II, footnote 17). It is unclear whether Digital Vertilog was commercially available as of 1991.

b. SoCalGas objects to this request as vague and ambiguous. Subject to and without waiving the foregoing objection, SoCalGas responds as follows. SoCalGas understands this request to seek Digital Vertilog records, not USIT records. See response to question 6a.

c. See response to question 6a.

QUESTION 7:

Prior to October 23, 2015, did SoCalGas run Vertilog, Digital Vertilog, USIT or HRVRT on SS-25?
a. If so, please provide the documentation showing this, including the logs and reports.
b. If so, provide all internal Memos that discuss the application of the technologies and/or results of these inspections.
c. If not, why not.

RESPONSE 7:

No.

a. N/A.
b. N/A.
c. No diagnostic testing (e.g., temperature surveys and noise logs), weekly pressures, or well site inspections of SS-25 indicated a casing integrity issue which required a workover prior to October 23, 2015. Casing inspection logs such as Vertilog, Digital Vertilog, USIT or HRVRT can only be performed in the course of a workover. No well rig work was required on SS-25 prior to October 23, 2015. As such, Vertilog, Digital Vertilog, USIT and HRVRT were not run on SS-25.

Blade's response to SED-DR-058, q. 1.2

2 Statements and Responses

2.1 Statement 1

Pages 1 and 2: "[Public Advocates Office's] allegations presuppose that the Vertilog technology at that time [1988] was reliable and accurate. That is not the case."

2.1.1 Blade Response

1. Does Blade Energy Partners agree or disagree with the statement?

   Disagree.

2. If Blade disagrees with any portion of the statement, why?

   The Vertilog or equivalent technology that existed in 1988 was capable of detecting and discriminating metal loss features, with only its sizing and characterization capabilities being limited compared to the current technology. That being said, it was the best technology available at the time for monitoring metal loss in casing and was sufficient to indicate the presence of corrosion issues.

   Mr. Carnahan incorrectly references a quote [page 2, line 12] found in a Pipeline & Gas Journal article (footnote #9). The original quote, which is related to pipeline inspection, is being misapplied to downhole logging. The complete quote is:

   > "Historically, the results of the first-generation MFL tools were not very satisfactory, but BG (British Gas) and then PII developed advanced electronics and analysis algorithms and software which set new standards in the industry."

   In Mr. Carnahan's testimony [at page 2, line 12, and page 8, line 13], he modifies the quote as follows:

   > "Historically, however, the results of the first generation of MFL tools were not very satisfactory.[9]"

   The original quotation notes the advances in technology but were not acknowledged by Mr. Carnahan. The statement by Goedecke, the original author, about first-generation magnetic flux leakage (MFL) tools and subsequent advances in technology was in reference to pipeline inspection tools. These first-generation MFL tools were developed from approximately 1959–1965 [1, 2, 3]. The first commercial effort to collect information using MFL tools was by AMF Tuboscope in 1965; the name of the tool was the Linalog [1, 2, 3]. By 1983, 112,000 km of pipeline had been inspected [4]. Mr. Carnahan mischaracterizes the Vertilog as a first-generation MFL tool but there were significant advances in MFL technology that began in the pipeline industry [2] prior to the Vertilog's deployment into oil and gas wells in the mid 1970's.

   Mr. Carnahan negatively portrays the Vertilog [page 2, line 8], "… as a mechanism that attempts to utilize Magnetic Flux Leakage (MFL) to detect casing metal loss[8]." The footnote #8 that Mr. Carnahan refers to was a 1977 Society of Petroleum (SPE) paper [5] written by employees of the logging company Dresser Atlas, which would later become part of Baker Hughes. The word "*attempts*" is not used in the reference. Although Mr. Carnahan describes the working principles of the Vertilog, he fails to provide the context that MFL and eddy current technology for the use of corrosion inspection were well established in oil and gas pipeline operations. The SPE paper's authors describe the Vertilog tool as follows:

CalAdvocates - 594

It is a quantitative measurement of corrosive damage, indicating if the metal loss is internal or external, and if it is isolated or circumferential. Holes in the casing can be identified as well as parted casing. This survey in conjunction with other measurements, can be used to detect, monitor, and establish preventive techniques for corrosive problems.

Figure 1 shows the Vertilog and Digital Vertilog (DVRT) performance specifications as of 1991 (provided by Mr. Rod Foster, Well Integrity Senior Advisor, Baker Hughes). The two tools are essentially the same tool and sensor system but the DVRT has upgraded electronics for improved acquisition and computerized processing [6]. The DVRT was deployed in approximately 1991, superseding the Vertilog. As a point of reference, the DVRT was considered by Blade[i] for use in logging of the 11 3/4 in. surface casing as part of the SS-25 RCA. Considering the wall thickness of 0.317 in. (for 7 in. 23 ppf production casing in SS-25), the Vertilog and DVRT could detect defects deeper than 30% or 0.095 in. and size them +/- 15% or 0.048 in. For the Vertilog and DVRT, a 50% deep defect could be sized between 35–65%. In comparison, the High Resolution Vertilog (HRVRT) can detect defects that are deeper than 15% or 0.048 in. and size them +/- 10% or 0.032 in. For the HRVRT, a 50% deep defect could be sized between 40-60%.

Measurement Range:	30 to 90% penetration of the casing wall in single string
Absolute Accuracy:	$\pm 15\%$ of actual pit depth in single string casing for isolated pitting, when casing information such as weight, grade, etc. is available
Repeatability:	$\pm 10\%$ of first reading if pipe was fully magnetized on first pass
Sensitivity:	Casing defects as small as 0.375 in. (9.5 mm) in diameter with as little as 30% penetration can be detected and recorded at 100 ft/min (30.5 m/min) in single string
Radial Investigation:	Tool is designed to inspect the full casing circumference
Depth of Investigation:	100% of the wall of the inside casing

Figure 1: Performance Specifications for the Vertilog, and Digital Vertilog from 1991

Table 1 shows a listing of casing inspection logs that were downloaded from the DOGGR website [7] during the course of Blade's RCA; the logs are within 10 years of the proposed dates of the 1988 Interoffice Correspondence 2-year logging program [8]. As discussed in Blade's Main RCA report [9, p. 204], Blade's position is that SoCalGas made a recommendation to run the Vertilog in 20 wells that concerned them at the time. Blade reviewed the logs listed in the table that were run in approximately the same time frame as the 1988 Interoffice Correspondence. Although we did not perform an exhaustive study; in our opinion, the Vertilog was superior to the inspection tools of its day, specifically, the Welex Casing Inspection Log, McCullough Electronic Casing Caliper, and Schlumberger Electromagnetic Thickness Log. The recommendation to run Vertilog casing inspections in 20 wells appeared to Blade to have been based on using the best available technology at that time for the purpose of assessing the mechanical condition of casing flow wells completed in the 1940s and 1950s.

---

[i] In 2016–2017, the DVRT was the was only MFL tool available to inspect the 11 3/4 in. casing. Although the sensor system was developed in the mid-1970's with upgraded electronics in approximately 1991, the DVRT was still in-service and was initially Blade's primary MFL logging option. Because it was important to attain the most accurate data, Blade requested that Baker Hughes and its vendor, Microline Technology Corporation, adapt the HRVRT to 11 3/4 in. casing size. The DVRT was not used in the SS-25 RCA.

Mr. Carnahan's assertion is that the Vertilog was unreliable and inaccurate and combined with other factors, would not have prevented the SS-25 incident. His basis for finding the Vertilog unreliable and inaccurate is derived from his numerical comparison of five (5) Vertilogs from 1988–1990 to various HRVRT and USIT logs run in 2013 and 2016–2018. This is an approach that would not have been available to SoCalGas in the late 1980s or early 1990s. Certainly, logging technology of 2010s would be expected to be more accurate than that of late 1980s and early 1990s. However, this does not mean that the older logging tools did not provide useful or actionable information.

For example, in 1989, researchers evaluated four types of casing inspection tools, stating the following [10]:

> Electromagnetic casing inspection logs are commonly used in the industry to survey the condition of casing. Logs may be used to estimate the amount of pitting, degree of corrosion, wall thinning, changes in diameter, and other casing features. Occasionally, casing inspection logs are used to investigate a casing failure in a well. Interpretations of casing inspection logs may be used to determine the type of remedial work on a well where a casing failure has occurred, or they may be an important factor in a commercial casing failure claim.

There are key concepts in this paper related to casing inspection tools available in 1989. The first was that casing inspection tools were commonly used for detecting pitting, degree of corrosion, and wall thinning. The second was the authors describe MFL technology, specifically mentioning the Vertilog, as capable of being able to distinguish between split and parted casing.

Two of the wells in Table 1 had underground blowouts, namely F-3 and FF-34A, which were logged in 1986 and 1991 respectively. These dates bookend the Vertilog logging campaign outlined in the 1988 Interoffice Correspondence. Note that the Schlumberger Ultrasonic Imager (USIT) was run in P-42B in 1993, which was not that long after the September 10, 1990 FF-34A casing failure and when the Vertilog logging campaign was discontinued.

Table 1: Aliso Canyon Casing Inspection Logs within 10 years of 1988–1990

Well	Date	Vendor	Log Name
FF-35B	August 31, 1978	McCullough	Electronic Casing Caliper
SS-1	February 27, 1980	McCullough	Electronic Casing Caliper
MA-1A	February 28, 1985	McCullough	Electronic Casing Caliper
F-3 [b]	January 31, 1986	Welex	Casing Inspection Log
F-4 [a c]	September 6, 1988	Western Atlas	Vertilog
P-37 [a]	October 11, 1988	Western Atlas	Vertilog
P-46 [a, c]	October 19, 1988	Western Atlas	Vertilog
SS-9 [a, c]	December 16, 1988	Western Atlas	Vertilog
SS-8 [a, c]	January 17, 1989	Western Atlas	Vertilog
P-32C	July 26, 1989	Western Atlas	Vertilog
P-34 [a, d]	November 2, 1989	Western Atlas	Vertilog
FF-35B [c, d]	November 11, 1989	Western Atlas	Vertilog
MA-1A	December 27, 1989	Western Atlas	Vertilog
F-2 [a, d]	January 11, 1990	Western Atlas	Vertilog

Well	Date	Vendor	Log Name
FF-35C	September 18, 1990	Western Atlas	Vertilog
SS-14	March 5, 1991	Halliburton	Casing Inspection Log
FF-34A [b]	May 11, 1991	Schlumberger	Electromagnetic Thickness Log
P-42B	January 11, 1993	Schlumberger	Ultrasonic Imaging Tool
P-68B	May 27, 1993	Halliburton	Casing Inspection Log
SS-14	May 26, 1998	Halliburton	Casing Inspection Log
SF-2	November 19, 1999	Schlumberger	Ultrasonic Imaging Tool

[a] – Wells listed in the 1988 Memo (F-4, P-37, P-46, SS-9, SS-8, P-34, F-2)

[b] – Wells that had blowouts (F-3, FF-34A)

[c] – Wells reviewed by Mr. Carnahan (F-4, P-46, SS-9, SS-8, FF-35B)

[d] – Logs not available on the DOGGR website (P-34, FF-35B, F-2)

Mr. Carnahan's spreadsheet analysis neglects important findings that are visible graphically on the log. There is considerable information that can be derived from looking at the log image. Different logs employ different technology; the characterization and sizing of features may appear different. Most logging companies have some version of the cement bond log with variable density (CBL – VDL) for the determination of zonal isolation (i.e., to evaluate if the cement is an effective barrier). Although these logs have been utilized for over 50 years, the best way to interpret the presence of cement and the bond to pipe and formation is to *look* at the log. There are wavy, chevron, zigzag, and other patterns that have meaning. This is the same for the Vertilog and other casing inspection logs. There is data in the patterns.

Blade performed an analysis of F-4's 1988 Vertilog as part of the RCA [11] comparing it to the 2016 Ultrasonic Imager (USIT) log. Figure 2 shows these two logs with the Vertilog on the left and USIT on the right. To aid in interpretation from joint to joint, the logs have been adjusted so that the casing connections of each log are aligned. External metal loss is denoted by blue text at A, B, and C on the Vertilog's Flux Leak track, and by the same letter on the USIT's wall thickness track. At A-A, external metal loss is found just above a connection. At B-B, external metal loss is found approximately midway in the joint. At C-C, there is external metal loss below a connection. The point here is the two logs found the same defects.

There was good agreement between the logs at most depths. However, in some cases, the logs did not agree. It should not be assumed that the 2016 USIT log was the more accurate one. In Blade's experience, MFL tools are better at detecting pitting corrosion. In general, it's a flawed concept to compare one log tool to another and automatically claim one is more accurate than the other. Log data has to be compared to truth data (direct measurements of defects) to assess log performance. In today's era, repeatability and reproducibility of pipeline inspection tools are verified independently in pull-through tests (e.g., Pipeline Research Council International Integrity and Inspection projects). Even today, very little data has been published in testing downhole logging tools in controlled environments. An independent comparison of casing inspection logging tools spanning decades does not exist, however, the Vertilog and other casing inspection tools could have been used as an indicator of an issue.
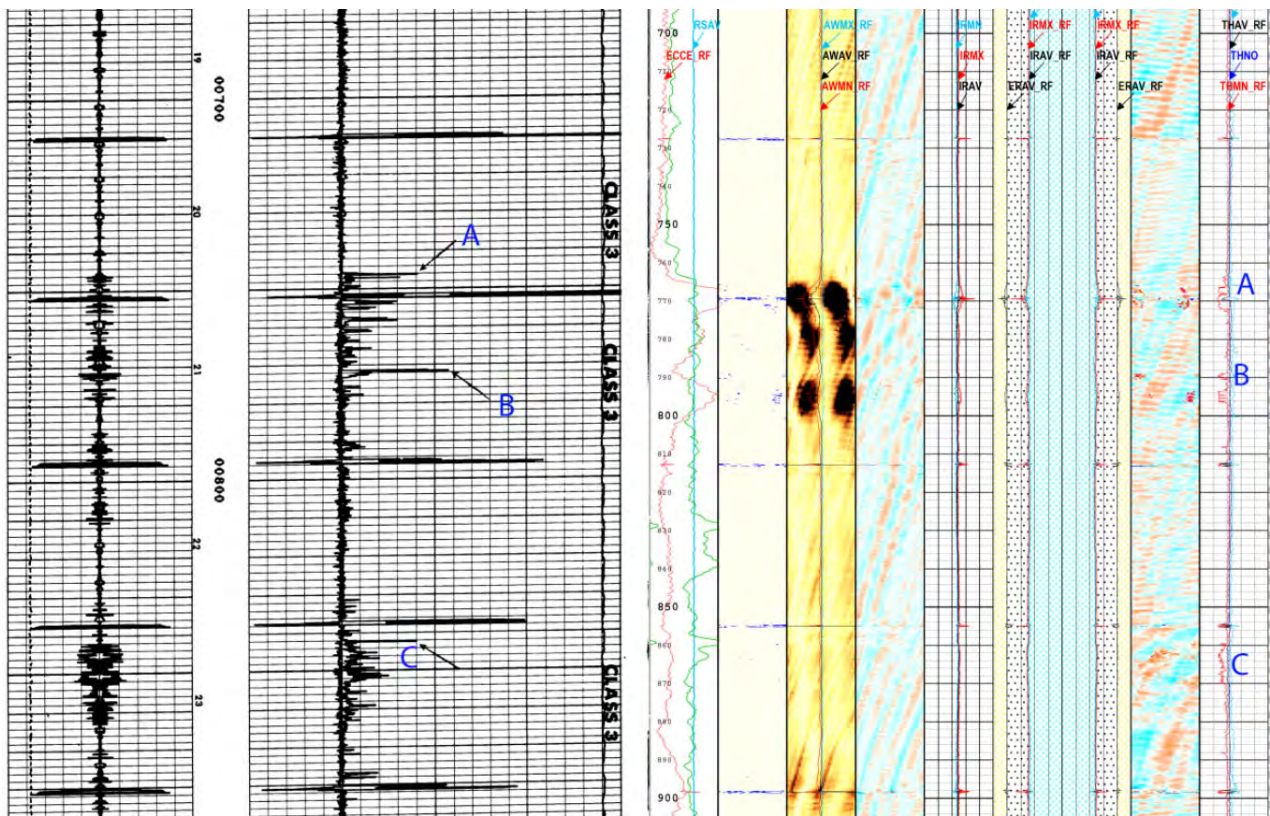
Figure 2: F-4 1988 Vertilog (Left) and 2016 USIT (Right) Comparison

3. Is there any context either in or outside of Mr. Carnahan's testimony that Blade wishes to add in order to explain its answers? If so, please provide it and explain.

SoCalGas had a two-year plan in 1988 to determine the mechanical condition of the casing in 20 wells originally completed in the 1940s and 1950s. Blade reviewed the records of all 20 wells to evaluate subsequent casing inspections and the casing problems that occurred in the following years. A number of casing problems were identified. SoCalGas made a recommendation to run casing inspection logs in 20 wells that concerned them at the time, and the opportunity to inspect the casing in SS-25 was missed. There is no way to know what an inspection of the SS-25 casing would have shown in 1988, but it is possible that corrosion was present and detectable, and steps could have been taken to avoid the leak in 2015 [9, pp. 2, 160, 173–181, 204-205] [12].

The fact is that SS-25 and other 1988 Interoffice Correspondence wells did not get inspected according to plan.

4. If Blade accepts any part of the statement as true, does it change any of the conclusions Blade reached in its Root Cause Analysis?

Even if Blade accepted Mr. Carnahan's statement as true, it would not change any of the conclusions Blade reached in its Root Cause Analysis.

5. If the answer to question 3 is yes, which conclusions change and what must they say now?

Not Applicable. No conclusion changes are needed.

[www.glossary.oilfield.slb.com/en/Terms/c/ casing-inspection_log.aspx](http://www.glossary.oilfield.slb.com/en/Terms/c/casing-inspection_log.aspx)
Schlumberger's Definition
of Casing Inspection Log

- Services & Products
- About Us
- Investors
- Newsroom
- HSE
- Careers
- Alumni
- Resources

Oilfield Glossary

Oilfield Glossary

Search for Term:

Language:

⦿ English ◯ Español [Search]

Search by Discipline

[All Disciplines ▾] [Go]

More search options

Terms beginning with:

#	A	B	C	D	E	F
G	H	I	J	K	L	M
N	O	P	Q	R	S	T
U	V	W	X	Y	Z	

Resource Links

Schlumberger Oilfield Services
Oilfield Review
Global Stewardship

Credits and Administration

Schlumberger Oilfield Glossary Credits
Glossary Administration

Tools

Print   Share

casing-inspection log

English | Español

1. n. [Production Logging]

An in situ record of casing thickness and integrity, to determine whether and to what extent the casing has undergone corrosion. The term refers to an individual measurement, or a combination of measurements using acoustic, electrical and mechanical techniques, to evaluate the casing thickness and other parameters. The log is usually presented with the basic measurements and an estimate of metal loss. It was first introduced in the early 1960s. Today the terms casing-evaluation log and pipe-inspection log are used synonymously.

See: casing-potential profile, eddy-current measurement

CalAdvocates - 600

www.slb.com/-/media/files/production/product-sheet/usi

Schlumberger's Product Description of USIT

USI UltraSonic Imager Tool
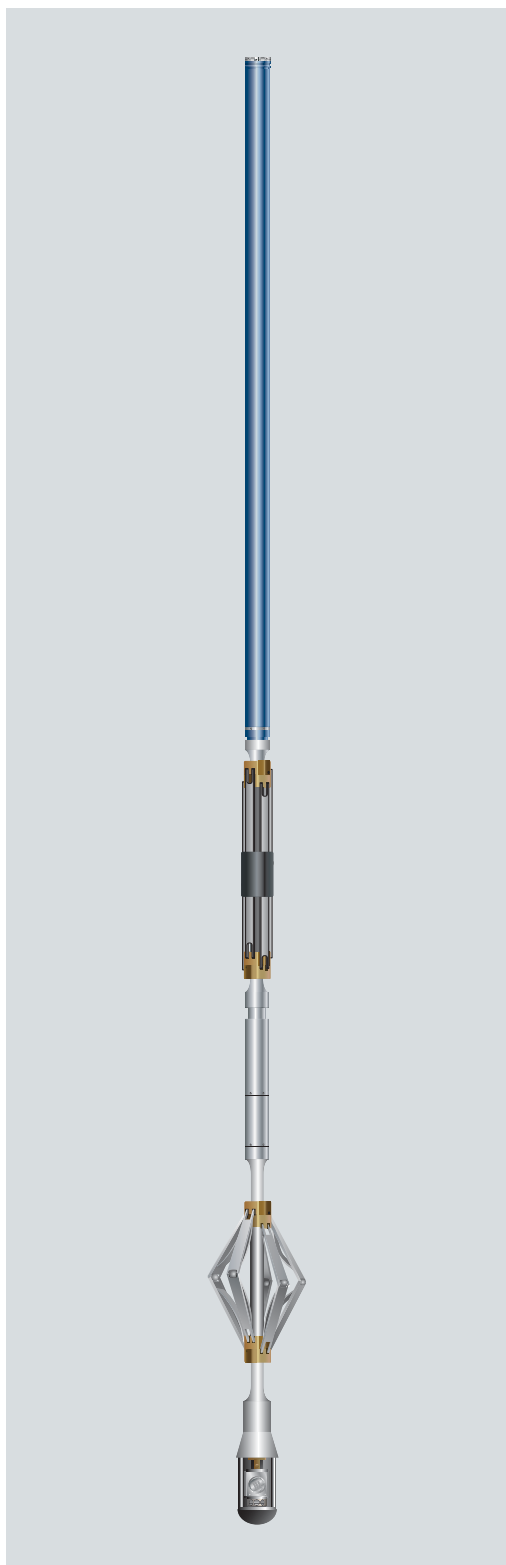
The USI* UltraSonic Imager tool (USIT) uses a single transducer mounted on an Ultrasonic Rotating Sub (USRS) on the bottom of the tool. The transmitter emits ultrasonic pulses between 200 and 700 kHz and measures the received ultrasonic waveforms reflected from the internal and external casing interfaces. The rate of decay of the waveforms received indicates the quality of the cement bond at the cement/casing interface, and the resonant frequency of the casing provides the casing wall thickness required for pipe inspection. Because the transducer is mounted on the rotating sub, the entire circumference of the casing is scanned. This 360° data coverage enables the evaluation of the quality of the cement bond as well as the determination of the internal and external casing condition. The very high angular and vertical resolutions can detect channels as narrow as 1.2 in. [3.05 cm]. Cement bond, thickness, internal and external radii, and self-explanatory maps are generated in real time at the wellsite.

Applications

- Cement evaluation
- Casing inspection
  - Corrosion detection and monitoring
  - Detection of internal and external damage or deformation
  - Casing thickness analysis for collapse and burst pressure calculations

Measurement Specifications

	USIT
Output	Acoustic impedance, cement bonding to casing, internal radius, casing thickness
Logging speed	1,800 ft/hr [549 m/h]
Range of measurement	Acoustic impedance: 0 to 10 MRayl [0 to 10 MPa.s/m]
Vertical resolution	Standard: 6 in. [15.24 cm]
Accuracy	Less than 3.3 MRayl: ±0.5 MRayl
Depth of investigation	Casing-to-cement interface
Mud type or weight limitations[†]	Water-base mud: Up to 15.9 lbm/gal Oil-base mud: Up to 11.2 lbm/gal
Combinability	Bottom-only tool, combinable with most tools
Special applications	Identification and orientation of narrow channels

[†] Exact value depends on the type of mud system and casing size.

Mechanical Specifications

	USIT
Temperature rating	350°F [177°C]
Pressure rating	20,000 psi [138 MPa]
Casing size—min.	4½ in. [11.43 cm]
Casing size—max.	13⅜ in. [33.97 cm]
Outer diameter[†]	3.375 in. [8.57 cm]
Length[†]	19.75 ft [6.02 m]
Weight[†]	333 lbm [151 kg]
Tension	40,000 lbf [177,930 N]
Compression	4,000 lbf [17,790 N]

[†] Excluding the rotating sub

USIT Rotating Sub Mechanical Specifications

	USRS-AB	USRS-A	USRS-B	USRS-C	USRS-D
Outer diameter	3.41 in. [8.66 cm]	3.58 in. [9.09 cm]	4.625 in. [11.75 cm]	6.625 in. [16.83 cm]	8.625 in. [21.91 cm]
Length	9.8 in. [24.89 cm]	9.92 in. [25.20 cm]	9.8 in. [24.89 cm]	8.3 in. [21.08 cm]	8.3 in. [21.08 cm]
Weight	7.7 lbm [3.5 kg]	7.7 lbm [3.5 kg]	10.6 lbm [4.8 Kg]	15.0 lbm [6.8 kg]	18.3 lbm [8.3 kg]

www.slb.com/oilfield

Schlumberger

www.glossary.oilfield.slb.com/en/Terms/f/flux_leakage.aspx
Schlumberger's Definition
of Flux Leakage

Search

- Services & Products
- About Us
- Investors
- Newsroom
- HSE
- Careers
- Alumni
- Resources

Oilfield Glossary

Oilfield Glossary

Search for Term:

Language:

◉ English ◯ Español [Search]

Search by Discipline

[All Disciplines ▾] [Go]

More search options

Terms beginning with:

#	A	B	C	D	E	F
G	H	I	J	K	L	M
N	O	P	Q	R	S	T
U	V	W	X	Y	Z	

Resource Links

Schlumberger Oilfield Services
Oilfield Review
Global Stewardship

Credits and Administration

Schlumberger Oilfield Glossary Credits
Glossary Administration

Tools

Print   Share

flux leakage

English | Español

1. n. [Production Logging]

A distortion of the magnetic flux that has been introduced into a casing by a low-frequency electromagnet or permanent magnet. The principle of flux leakage is used to detect casing corrosion, since flux leakage is caused by rapid changes in the thickness of the casing and by pits and holes in either the internal or external wall. Flux leakage distorts the magnetic-flux lines and induces a signal into an electric coil moving past it. In-situ flux-leakage measurements make use of this effect by placing coils on or close to the casing wall, azimuthally distributed to cover the entire wall. The results are often combined with a high-frequency, eddy-current measurement, designed to detect flaws only on the inner wall.

See: azimuthal, casing-inspection log, casing-potential profile, eddy current, eddy-current measurement, pitting

A. J. Hayman, R. Hutin, and P. V. Wright, *High-Resolution Cementation and Corrosion Imaging By Ultrasound* (1991)

HIGH-RESOLUTION CEMENTATION AND CORROSION IMAGING BY ULTRASOUND

A. J. Hayman, R. Hutin, and P. V. Wright*

Schlumberger

April 2, 1991

Abstract

The UltraSonic Imager (USI[1]) tool is a new wireline tool for cement evaluation and corrosion detection by ultrasonics. A rotating ultrasonic transducer gives full coverage of the casing at high resolution. The principle is similar to existing ultrasonic tools: the transducer emits a short pulse which excites a thickness-mode resonance in the casing. Analysis of the echo gives four measurements: internal radius, rugosity, casing thickness and cement acoustic impedance. The cement impedance indicates cement quality and presence. Good cement has higher impedance than poor cement or drilling fluids.

The internal radius and rugosity are derived from the travel time and amplitude of the main echo using a technique that eliminates cycle-skipping problems. The casing thickness and cement impedance are measured by a novel signal-processing algorithm that matches a theoretical model to the measured resonance in the frequency domain. The processing corrects for the effects of casing thickness variations, mud attenuation and transducer variations on the cement impedance. Mud variations are compensated by measuring the mud velocity and impedance downhole.

Field results show that channeling, contaminated cement, light cement and gas can be diagnosed and that external hardware such as centralizers can be detected. The corrosion measurements can detect mechanical wear, corrosion and deposits.

1 Introduction

There are two widely used methods of cementation evalution: the sonic and ultrasonic techniques.

The sonic method, first developed about 30 years ago [1], measures the attenuation of a compression wave of about 20-kHz frequency propagating in the casing and along its axis. The wave loses energy mainly through shear coupling to the surrounding cement, so that well-bonded solid cement attenuates more strongly than a fluid outside the casing.

Two major problems arise with the sonic technique. First, the lack of azimuthal resolution makes it difficult to distinguish channeling from poor cement. Second, microannulus removes

KK

1

the shear coupling and gives a response similar to fluid behind the casing. Reflections from hard formations or second casing strings [4,5] and early arrivals through "fast" formations pose additional problems and often invalidate the measurements.

Improved methods of qualitative interpretation and new environmentally compensated tool designs [2] were developed over the years, but the resolution and microannulus limitations remained. Recently a prototype sonic tool using sectored transmitters and receivers to obtain 45° azimuthal sampling was described [3], and another with 6 pairs of transducers and receivers has been developed commercially.

The sonic type of measurement does have certain advantages, including the positive response to solid cement, a qualitative indication of the cement-to-formation bond from the waveform display, and the ability to operate in most well fluids.

The ultrasonic pulse-echo method was developed to combat the limitations of the sonic method. The basic idea is to set up a thickness-mode resonance in the casing: good cement damps the resonance while poor cement or mud gives a slower decay. The first ultrasonic tool, the Cement Evaluation Tool (CET[1]), comprises 8 transducers arranged to give 45° sampling [6]. Each transducer has a resolution of about 30 mm. Because the wave motion is normal to the casing wall, shear coupling is unimportant and microannulus has relatively little effect compared to the sonic method. Formation reflections are detected and often compensated by the CET signal processing. The ultrasonic method also provides extra information about the casing geometry for corrosion and damage evaluation [7].

Chief limitations of the ultrasonic method are twofold: first, lightweight and gaseous cements have low contrast from well fluids, and second, operation in heavy muds is restricted because of attenuation of the relatively high-frequency ultrasound. Therefore, the ultrasonic method has complemented rather than supplanted the sonic method [8].

This paper describes a second-generation ultrasonic tool incorporating the following new features:

- Full coverage of the casing at high resolution using a rotating transducer.

- Digital technology to record all waveforms and send them to the surface for processing.

- A novel model-based signal-processing method that is less sensitive to environmental effects.

- Capability to operate in heavier muds.

- Color images of cementation and corrosion measurements.

2 Principle

2.1 Measurements

The heart of the USI tool is a rotating ultrasonic transducer immersed in the drilling fluid, which gives full coverage of the casing at high resolution. The transducer excites the casing resonance by repeatedly emitting short pulses of ultrasound (Figure 1) at normal incidence to the casing, and the same transducer operated as a receiver detects the echoes from the casing.

Four measurements are made by analysis of the echoes:

1. **Echo amplitude** – an indicator of casing condition.

2

Table 1: Acoustic properties of materials

Material	Density ($\mathrm{kg.m^{-3}}$)	Acoustic velocity ($\mathrm{m.s^{-1}}$)	Acoustic impedance (MRayl)
Air (1–100 bar)	1.3–130	330	0.0004–0.04
Water	1000	1500	1.5
Drilling fluids	1000–2000	1300–1800	1.5–3.0
Cement slurries	1000–2000	1800–1500	1.8–3.0
Cement (Litefil)	1400	2200–2600	3.1–3.6
Cement (class G)	1900	2700–3700	5.0–7.0
Limestone	2700	5500	17
Steel	7800	5900	46

2. **Internal radius** – calculated from the transit time of the echo.

3. **Casing thickness** – calculated from the resonant frequency.

4. **Acoustic impedance** of the material behind the casing – calculated from the form of the resonance.

The cement evaluation is based on an acoustic impedance measurement. In a homogeneous nondissipative medium, the acoustic impedance Z is equal to the product of the density ρ and acoustic velocity v:

$$Z = \rho v. \tag{1}$$

Acoustic impedances are commonly expressed in units of MRayl (1 Rayl = 1 $\mathrm{kg.m^{-2}.s^{-1}}$). The acoustic properties of some materials encountered in oil wells are listed in Table 1.

2.2 Impulse Response: Plane-Wave Model

The essential physics of the USI tool can be understood by assuming the ultrasonic wave to be plane and incident normally on a flat plate representing the casing. Figure 1 shows the wave propagation and the impulse response. Most of the incident energy is reflected at the mud-casing interface, because of the large impedance contrast between the mud and steel. The small fraction of the energy transmitted into the casing is multiply reflected in its thickness, releasing a transmitted pulse into the cement or mud each time it strikes a casing surface.

Thus the impulse response consists of a large initial reflection from the internal surface of the casing followed by an exponentially decaying series of inverted impulses. The time of arival of the initial reflection is $2S/v_{mud}$, where S is the standoff from transducer to casing and v_{mud} is the acoustic velocity in the mud.

The time separation of the train of negative impulses is equal to the go-and-return time in the casing:

KK

$$\Delta t = 2d/v_{steel}, \tag{2}$$

where d is the casing thickness and v_{steel} the velocity in steel.

3

The amplitudes of the impulses depend upon the acoustic impedances of the mud, steel and cement. Figure 2 shows three impulse responses plotted on a dB scale, where the exponential decay becomes a linear decay. A measurement of the echo amplitude after many reflections provides maximum sensitivity to cement impedance and minimum sensitivity to mud impedance. However, after many reflections on cement, the amplitude is very small (-50 dB after 10 reflections), so the signal-to-noise ratio is poor and the signal cannot be digitized accurately. There is also the problem of formation reflections corrupting the later part of the signal. For these reasons the USI processing analyzes the early part of the signal where there is a good signal-to-noise ratio.

2.3 Fundamental Frequency Operation

To minimize attenuation in weighted drilling muds, the transducer is operated at the lowest possible frequency: the fundamental resonant frequency $f_0 = 1/\Delta t$. There are two additional reasons for preferring the fundamental over higher harmonics: first, because the fundamental mode decays slower than higher harmonics in a cylindrical casing, leading to a higher signal-to-noise ratio, and second, because the lower-frequency mode is less sensitive to casing profile and rugosity.

The normal range of casing thicknesses (4.5 to 15 mm) corresponds to a fundamental frequency range of 0.65 to 0.19 MHz. To cover this wide range, one of two transducers of overlapping bandwidth is used: a high-frequency transducer for thin casings or a low-frequency transducer for thick casings (Figure 3). The transducers have been designed to provide short well-damped pulses so as not to interfere with the casing resonance.

The echo from the casing is the convolution of the transducer response with the casing impulse response, so it consists of a large initial echo followed by a decaying resonance, as shown in Figure 4. The initial echo is out of scale and is actually four times larger than plotted.

3 Signal Processing: T^3

The USI signal-processing method is called T^3 (*Traitement Très Tôt* = Very Early Processing), because it analyzes the early part of the resonance.

3.1 Model-Based Approach

T^3 fits a model to the measured signal. In the interests of processing speed, the simple plane-wave model (Figure 1) is used. This model incorporates five important parameters: the acoustic impedances of the mud, steel and cement, plus the casing thickness and the acoustic velocity in the steel. Now the steel impedance and velocity are known, and the mud impedance is measured separately (Section 4.1), so there remain two parameters to be adjusted in the model: the cement impedance and the casing thickness.

3.2 T^3 Algorithm

The algorithm has five principal steps.

4

Step 1: Peak location

The time of arrival and amplitude of the initial echo are estimated by fitting a quadratic polynomial through the three adjacent, maximum absolute-magnitude peaks of the waveform (Figure 5). This algorithm is very stable and completely eliminates the problem of cycle-skipping.

Step 2: Normalization window

A very short normalization window (Figure 6) is used to select the initial reflection substantially unaffected by the casing resonance. This represents the approximate system response (transducer, electronics and propagation through mud). The frequency spectrum of this signal, the normalization spectrum, is inserted in the model in step 4 to automatically compensate for spectral variations caused by mud attenuation or by transducer variations with temperature and pressure.

Step 3: Process window

The "process" window (Figure 6) selects the initial reflection and the early part of the resonance for analysis. The duration of the process window has been minimized for several reasons: to avoid formation reflections, to improve the signal-to-noise ratio and digitization accuracy, to reduce the data rate for uphole processing, and to permit a reduced standoff in order to reduce signal attenuation in attenuative muds. The usual process window length (peak to end of window) is between 6 and 8 periods of resonance.

The fundamental resonance is found and characterized by frequency analysis of the process-windowed signal, using the group delay (the derivative of the phase with respect to the angular frequency). An example illustrates the advantages of using group delay. Figure 7 shows the frequency spectrum– amplitude, phase and group delay– of the windowed time signal from Figure 6. The amplitude spectrum has a broad peak representing the transducer frequency response, with small minima at the resonances: the fundamental resonance at approximately 0.35 MHz and the first harmonic at about 0.7 MHz. By contrast, the group delay is almost flat except at the resonances, which produce clear minima.

The resonance is found by searching for the group delay minimum in a preselected range around the expected frequency. The resonance dip (Figure 8) is characterized by its resonant frequency f_0 and its fractional bandwidth $\Delta f / f_0$.

Step 4: Calculation and characterization of model response

1. Estimate the casing thickness from the measured resonant frequency, and estimate the cement impedance (the initial estimate is not critical).

2. Calculate a model waveform using the normalization spectrum and the estimated thickness and impedance.

KK

3. Apply the process window and calculate the group-delay spectrum.

4. Measure the resonant frequency and fractional bandwidth of the modeled resonance.

Step 5: Model iteration

The resonant frequency and fractional bandwidth of the modeled resonance are compared with those of the measured resonance. Then improved estimates for the cement impedance and thickness are calculated, and the model is recalculated. The procedure is iterated until the model and measurement match, which typically requires only three iterations. The outputs of the iteration are the cement impedance Z_{plane} and casing thickness d_{plane} which provide the best fit of the planar model to the measured echo.

4 Cement Impedance Measurement Method

T^3 processing determines the cement impedance that best fits the measured casing echo by theoretical modeling using the plane-wave model. Two supplementary pieces of information are needed to calculate an accurate cement impedance:

1. The acoustic properties (velocity and impedance) of the drilling fluid.

2. Corrections for the nonplanar geometry of the casing and transducer.

4.1 Fluid Properties Measurement

An accurate knowledge of the fluid properties inside the casing is essential to calculate the cement impedance outside. The mud impedance is an input to the T^3 model, while the velocity is needed to calculate the nonplanar correction (and to calculate the internal radius).

The transducer has two positions: Measurement, facing the casing, and Fluid Properties Measurement, facing a built-in target plate (Figure 9). The mud velocity is calculated from the transit time of the echo from the target; the impedance is determined by direct measurement using a special version of T^3 where the impedance is set equal on either side of the target. The fluid properties are measured while running into the well, and the sub is not rotated to avoid centrifuging solids onto the target.

As a check and alternative solution (for example, in case of fouling of the target by oil in a clear-fluid well), a separate impedance estimate is made using

$$Z_{mud} = \rho_{mud} v_{mud}. \tag{3}$$

The density ρ_{mud} is given by the driller (and corrected for temperature and pressure), and the measurement of the velocity v_{mud} is hardly affected by fouling. This approach is generally satisfactory for clear fluids.

The estimate is, however, less accurate in weighted muds for two reasons. First, laboratory measurements [11] have shown that the impedance of a weighted mud is less than $\rho_{mud} v_{mud}$ at ultrasonic frequencies, so a correction factor in the range of 0.8–1.0 must be applied. Second, a weighted mud may be vertically inhomogeneous due to inadequate circulation or sedimentation. This emphasizes the importance of the direct measurement of mud impedance.

4.2 Correction for Nonplanar Geometry

The "nonplanar" corrections are calculated by running the T^3 processing on waveforms created by an accurate 3-dimensional model [9,10]. Plotting the T^3 output Z_{plane} against the true impedance Z_{cemf} produces an almost linear impedance correction curve, like that shown in Figure 10. Note that the cement impedance is given in terms of fluid impedance Z_{cemf}.

6

5 Fluid/Solid Effect

The planar model makes no distinction between solids and fluids behind the casing, because only normal-incidence compression waves are included. In fact, the casing resonance is a superposition of complex resonances at small angles of incidence, which partially couple to shear waves in the casing and in the cement if the cement is solid and well-bonded to the casing. The additional damping provided by shear-wave coupling into the cement slightly increases the impedance measurement, as shown in Figure 11. Loss of shear coupling due to microannulus eliminates this small difference between solids and liquids (see Section 7.4).

6 Experiments: Impedance Measurement and Spatial Resolution

The USI principle and signal processing have been extensively tested in the laboratory and by theoretical modeling.

Figure 12 shows an experiment in a water-filled 7-in. diameter, 9-mm thick machined casing. The casing was cemented with 1900 kg.m^{-3} neat cement, and artificial channels were created using expanded polystyrene (Z=0 MRayl). The results comprise an initial scan with water outside, and further scans with the channels in place just after pouring the slurry, after 24 hours when the cement was solid, and after 5 days. There are two important features: first, even the smallest channel, 20 mm wide, is detected, and second, the measured cement impedance increases with time as the cement sets.

The spatial resolution of the measurement is defined as the minimum quantifiable channel (i.e., the smallest channel giving a reading equal to that from a large channel). Experimentally, the smallest quantifiable channel in casings from 4.5 in. to 13.375 in. in diameter has been found to be approximately 30 mm irrespective of diameter (Figure 12). The angular resolution thus improves proportionately with diameter, from about 30° in 4.5-in. casing to about 10° in 13.375-in. casing. This resolution is compatible with expected channel sizes and with the tool azimuthal sampling in cementation mode (10° or 5°). The vertical resolution is also about 30 mm.

7 Other Factors Affecting Impedance Measurement

7.1 Eccentering

Tool eccentering can be resolved into a change of standoff and a change in lateral position. The latter makes the beam arrive off normal incidence and is the major cause of error. In thin (5-mm) casings, eccentering errors are generally less than 0.5 MRayl when the eccentering is less than 0.5 mm/in. of casing diameter (2% of casing diameter). The tool centralizers keep eccentering within these limits.

In casings thicker than 5 mm, the eccentering errors are smaller. Figure 13 shows the effect of lateral eccentering in a typical case.

KK

7.2 Mud Properties

The fluid inside the casing poses two major problems: variations in impedance and high attenuation in weighted muds.

7

T^3 processing is sensitive to the amplitudes of the early multiple reflections, which in turn are very sensitive to the mud impedance (Figure 2). The solution is to measure the mud impedance downhole (Section 4.1).

The attenuation in weighted muds is approximately proportional to the frequency and increases linearly with mud density. Oil-base muds are roughly twice as attenuative as water-base muds of the same density. The selective loss of high frequencies shifts the frequency spectrum of the signal downwards. These changes in the shape of the spectrum are compensated by the T^3 normalization window. In addition, the frequency and form of the electrical firing pulse are modified when operating in attenuative muds in order to maximize the spectrum at the frequency of resonance.

7.3 Formation Reflections

One of the motivations for early processing was to minimize contamination by reflections from the formation or second casing string. A practical guideline for the minimum annulus thickness to avoid significant formation reflections from hard formations is $d_{cem} \geq 4dv_{cem}/v_{steel}$, so that neat cement must be about twice as thick as the casing, and a water annulus must be thicker than the casing.

Formation reflections, if present, can usually be detected on the cement map by a characteristic "galaxy" pattern of interference fringes, centered on the narrowest part of the cement sheath. Successive fringes indicate a change of one-half wavelength in the annulus thickness (Figure 14), where the wavelength λ is given by $\lambda = v_{cem}/f_0 \simeq 2v_{cem}d/v_{steel}$. For example, if there is neat cement behind a 9-mm thick casing, $\lambda/2 \simeq 5$ mm.

7.4 Microannulus

A microannulus is a small fluid-filled gap between the casing and cement. Figure 15 compares experiment and theory for a water microannulus behind a 7-in.-diameter, 6-mm thick casing cemented with 6 MRayl cement. The experiment was done by pulling a slightly conical casing vertically out of the cement. Initially, the measured impedance reads about 20% high because of the shear coupling to the cement (see Section 5). Once the bond between the casing and cement is broken, the small liquid-filled microannulus removes the shear coupling and brings the impedance down to the correct value. Further increases in microannulus gradually decrease the measured impedance. At 100 μm of microannulus it is still possible to distinguish water from cement, although the measured impedance is 50% low. Theoretical modeling predicts that microannulus has less effect behind thicker casings because of their lower resonant frequencies, as illustrated by the curve for 12-mm thickness.

A gas-filled microannulus always reads gas.

8   Acoustic Properties of Cement and Interpretation

An understanding of the acoustic properties of the cement and mud behind the casing is essential for a good interpretation of the USI acoustic impedance measurements.

Figure 16 shows typical acoustic properties of mud, cement slurry and cement (after 7 days or more cure at ambient conditions). The mud [11], slurry and some cement values were measured in our laboratory; others were measured by Jutten [12]. The rate of cure depends on the temperature and pressure, and on additives and type of cement.

8

The aim of the interpretation is usually to separate fluids from materials likely to provide hydraulic isolation, including poorly set and contaminated cement. In neat cement a cutoff can be defined above the maximum expected mud impedance, at 2.6 MRayl for a 1900 kg.m^{-3} cement. Lightweight cements are more difficult to distinguish from fluids because of their low impedances, so a qualitative interpretation and the combination with a sonic log are recommended. The problem of very light gas-contaminated cement, which can have an impedance between those of free gas and well fluids, is also best attacked by the sonic/ultrasonic combination.

9   Tool and Specifications

The USI tool consists of a sonde with a rotating transducer at the bottom (Figure 17), and a separate electronic cartridge situated above the sonde.

The transducer is housed in a rotating sub-assembly, or "sub," which is driven at 7 rps by a shaft connected to the motor inside the sonde. To optimize the distance from the transducer to the casing, five sub sizes are available to cover the casing size range from 4.5 to 13.325 in. Strong centralizers on the body of the sonde maintain good centralization even in horizontal wells.

The transducer has two positions: Fluid Properties Measurement, facing the built-in target plate, and Measurement, facing the casing. The transducer is flipped from one position to the other by reversing the sense of rotation.

The electronic emitter and preamplifier are situated very close to the transducer inside the rotating shaft, and the electrical connection to the sonde is made using a rotating transformer. The electronic cartridge synchronizes the transducer firing rate to the measured rotation speed. The signals are amplified, digitized and compressed before being sent to surface for real-time processing. All the waveforms are recorded for later analysis, if needed.

The tool specifications are shown in Table 2, and the logging modes are shown in Table 3. In cement mode the tool acquires cement and corrosion information. The corrosion modes provide higher resolution, but only corrosion information is recorded. The logging mode is selected from the surface and can be changed at any time.

10   Log Examples

The USI results are available in real time on a color monitor and color plotter. There are three standard presentations: a combined presentation showing cementation and corrosion information, and separate cement and corrosion presentations.

Example 1 shows a combined presentation. From left to right, the tracks are:

Track 1– Tool eccentering and eccentering azimuth calculated from the transit times.

Track 2– Processing and telemetry diagnostics.

Track 3– Map of amplitude relative to the maximum amplitude at the same depth. Dark shades indicate low amplitude. Maximum and minimum amplitude curves.

Track 4,5– Mean internal and external radius plus their mirror images. The external radius is the sum of the measured internal radius and the measured thickness. Minimum and maximum internal radius are also shown.

KK

Track 6– Map of internal radius relative to the mean at each depth, corrected for eccentering. Blue indicates smaller radii, and red larger.

9

Track 7– Thickness curves–min/mean/max.
Track 8– Map of thickness relative to the mean at each depth. Blue/red indicate thicker/thinner.

Track 9– Cement impedance map. Darker shades of brown show higher impedances.
Track 10– Gas index and bond index derived from the interpreted cement map. Gas (red) and bond (yellow) indexes represent the fraction of casing circumference surrounded by gas and cement, respectively; the remainder is classed as liquid (blue).
Track 11– Interpreted cement map where red, blue and yellow/brown indicate gas, liquid and solid. The impedance thresholds are typically less than 0.6 MRayl for gas and greater than 2.6 MRayl for neat cement.
Track 12– Acoustic casing collar locator.

Example 1: Channeling and casing wear

Channeling is obvious in the cement images on the right. This example comes from a 7-in., 23-lbm/ft test well where thousands of tools have been run over the years, and a groove worn by the wireline cable shows up on all the images. The diagnostics (track 2) indicate that the signal processing has been unable to measure the thickness and impedance along the narrow groove. The patterns on the thickness, internal radius and amplitude maps are characteristic of seamless (forged) casing.

Example 2: Channeling

A second example of channeling, behind a 7-in., 35-lbm/ft casing, is shown in the cement-only presentation, which includes the sonic measurements: the Cement Bond Log (CBL[1]) and the Variable Density[1] Log (VDL) waveform display (on the right). The CBL bond index (black line) agrees well with the USI index, but the CBL is incapable of diagnosing narrow channeling. In particular, the narrow channel in the center of the log, which gives 80% bond index, would be classed as an isolated zone by a CBL measurement alone.

Example 3: Formation reflections

This section of the test well contains a 7-in., 23-lbm/ft casing inside a 9.625-in. casing. The characteristic "galaxy" pattern of interference fringes caused by reflections from the second string through good cement is apparent along the narrow side of the annulus. Towards the top, a channel forms– a fairly common occurence because cement placement problems usually occur along the narrow part of the annulus.

Example 4: Scratchers

Scratchers (vertical lines) and centralizers (horizontal lines) can be seen in this good cement job, together with plugs of heavier cement. The 9.625-in., 36-lbm/ft casing was logged in Europe.

Example 5: Light cement, oil-base mud

Two sections of a light cement job (1500-kg.m^{-3} bentonite-extended cement) in a European well are shown. The USI cement threshold was reduced to 2 MRayl because of the low cement

10

impedance expected (<3.5 MRayl). The job was run in an oil-base mud of density 1030 kg.m^{-3} (8.6 lbm/gal).

The upper section shows the cement top where both the USI tool and the CBL are in good agreement. Note that both the USI impedance and CBL amplitude suffer reduced contrast in light cement.

The lower section shows part of the transition to the tail cement (1900 kg.m^{-3}) where a plug of higher-impedance cement is evident on the USI log. The regions of 100% heavy cement are indicated by low CBL amplitude (<2 mV), but the higher CBL readings are ambiguous. The USI images show both cement type and placement.

Example 6: Welded casing– contaminated cement, mud channels

Welded casing is common in North America where this 4.5-in., 9.5-lbm/ft casing was logged. The almost vertical blue lines on both the internal radius and thickness images from the USI log indicate that there is about 0.02 in. (0.5 mm) of untrimmed internal weld bead on all the casing joints but one. This poor trim affects the impedance measurement. The weld appears slanted because of a small amount of tool rotation.

The well was cemented using a light cement (13.5 lbm/gal) lead that gave surface returns, and the neat tail cement was designed to cover 2900–1400 ft. The logs were run in the tail cement zone.

In the lower section (2515–2410 ft), the USI, CET and CBL logs all show good cement plus intermittent channels. The CET map is in good agreement with the USI map taking into account a slight difference in tool rotation, and the CBL bond index (track 1) is consistent with the CET and USI indexes.

However, in the upper section (2250–1900 ft) the USI image shows contaminated cement, while the CET and CBL indicate 50% bond index; the CET map suggests contamination rather than channeling. The sonic bond index is meaningless in contaminated cement. Note that the USI response is unaffected by the thickness reduction in one joint.

Example 7: Gas problem

The client had gas coming to surface inside the casing in a ten-year-old gas well in Europe. The 9.625-in. casing was set at 1037 m, with a 7-in. liner from 1080 to 842 m. The USI log was run in a water-base mud of density 1410 kg.m^{-3} (11.7 lbm/gal).

The log of the 7-in. casing shows irregular patches of gas and good cement, with gas communication throughout. A narrow gas channel is apparent in the lower section reproduced here. The upper section shows the transition to the 9.625-in. casing where the cementation is excellent. Our interpretation of these results is that the initial cementation was good apart from a narrow gas communication channel (the well was cemented under gas pressure, and the CBL showed near 100% cement). With time the cement has become unbonded from the 7-in. liner, creating a gas microannulus through which the gas escapes to the inside of the 9.625-in. casing.

KK

Example 8: Generalized Corrosion

This example from a geothermal well in the suburbs of Paris is shown in corrosion-only presentation. Logs were recorded before and after cleaning the well. In the first run (top), internal

11

deposits of up to 0.1 in. were apparent from the internal radius measurements. The thickness measurement indicated about 30% metal loss compared to nominal (shown by a dotted line), but the measurement was rather noisy in the area of the deposits. Since the true internal radius of the casing could not be measured, the external radius (internal radius plus thickness) was not plotted.

The second run (bottom) shows that the cleaning operation was successful, for the deposits have disappeared. The thickness patterns characteristic of forged pipe are still evident after 30% metal loss, so the corrosion is quite uniform.

The ranges of color scales used for these images are widened compared to the previous cementation examples, for there is greater variability in amplitude, radius and thickness. Corrosion images are usually plotted with absolute scales rather than the relative scales used in this example, in order to indicate, for example, thickness loss from nominal.

11 Conclusions

The USI tool provides improved accuracy, resolution and coverage for both cementation and corrosion measurements compared to existing ultrasonic tools. For cementation, the signal processing compensates for thickness changes and mud attenuation, and reduces sensitivity to formation reflections, while the downhole fluid properties measurement compensates for mud impedance variations. Operation in heavier muds is possible. The color images at high resolution enhance the interpretation. Field results show that the cementation measurement can detect channeling, contaminated cement, light cement, gas and external hardware, while the corrosion measurements can detect mechanical damage, corrosion and deposits.

Acknowledgments

We would like to thank the many colleagues in Clamart and other Schlumberger centers who have contributed to this project, and in particular G. Rouault, who processed the data and produced the images. We are grateful to the oil and gas companies for permission to publish the logs. The corrosion example is by courtesy of GPC and AFME.

References

[1] G. H. Pardue, R. L. Morris, L. H. Gollwitzer and J. H. Moran, "Cement Bond Log – A Study of Cement and Casing Variables," *J. Pet. Tech.*, May 1963, 545-55.

[2] L. H. Gollwitzer and J. P. Masson, "The Cement Bond Tool," 23rd SPWLA Symposium, July 1982.

[3] M. G. Schmidt, "The Micro CBL – A Second Generation Radial Cement Evaluation Instrument," 30th SPWLA Symposium, June 1989.

[4] J. J. Jutten, "Relationship between Cement Bond Log Output and Borehole Geometrical Parameters," SPE/IADC 16139, New Orleans, March 15–18, 1987.

[5] J. J. Jutten, "Studies with Narrow Cement Thicknesses Lead to Improved CBL in Concentric Casings," SPE 18028, Houston, Oct. 2–5, 1988.

[6] B. Froelich, D. Pittman and B. Seeman, "Cement Evaluation Tool – A New Approach to Cement Evaluation," SPE 1027, San Antonio, Oct. 5–7, 1983.

12

[7] A. Dumont, J-B. Patin and G. LeFloch, "A Single Tool for Corrosion and Cement Evaluation," SPE 13140, Houston, Sept. 1984.

[8] G. N. Catala , I. D. Stowe and D J. Henry, "A Combination of Acoustic Measurements to Evaluate Cementations," SPE 13139, Houston, Sept. 1984.

[9] C. J. Randall and F. E. Stanke, "Mathematical model for internal ultrasonic inspection of cylindrically layered structures," *J. Acoust. Soc. Am.*, **83**, 4, 1295-1305,(1988).

[10] F. E. Stanke, C. J. Randall, and R. D'Angelo, "Experimental verification of mathematical model for internal ultrasonic inspection of pipes," *J. Acoust. Soc. Am.*, **88**, 1, 525–534,(1990).

[11] A. J. Hayman, "Ultrasonic Properties of Oil-Well Drilling Fluids," *Proc. 1989 IEEE Ultrasonics Symposium*, Montreal, Canada, Paper PE-1, 327–332 (IEEE, New York).

[12] J. Jutten, D. Guillot and P. Parcevaux, "Relationships between Cement Slurry Composition, Mechanical Properties and Cement Bond Log Output," SPE 16652, 1987.

About the authors

Andrew Hayman   *Remi Hutin*   *Peter Wright*
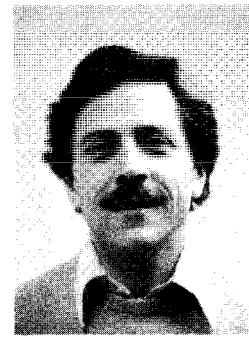
Andrew Hayman has a B.Sc. from the University of Bristol, an M.Sc. from the University of Aberdeen, and a Ph.D. in physics from The City University, London. After ultrasonics research at Université Paris 7, he worked on non-destructive testing for British Steel in Corby, U.K. In 1985, he joined Etudes et Productions Schlumberger in Clamart, France, where he has specialised in ultrasonic cement evaluation.

Remi Hutin has an engineering degree from the Ecole Supérieure d'Electricite near Paris. From 1975 to 1978, he worked on radar design at Thomson CSF. In 1979, he joined Schlumberger in Clamart where he has participated in the design of several wireline tools, as an engineer and later as a project manager. He has been the manager of the USI project since 1987.

Peter Wright graduated from Churchill College, Cambridge. He began his career in the microwave industry, first in the U.K. and then in the U.S.A. After obtaining a doctorate from MIT, he worked on Surface-Acoustic-Wave devices at Lincoln Laboratories, Lexington, MA, and at RF Monolithics Inc., Dallas, TX. He developed the signal-processing algorithm for the USI while working for Schlumberger in Clamart from 1986-1989. He has now returned to RF Monolithics.

KK

13
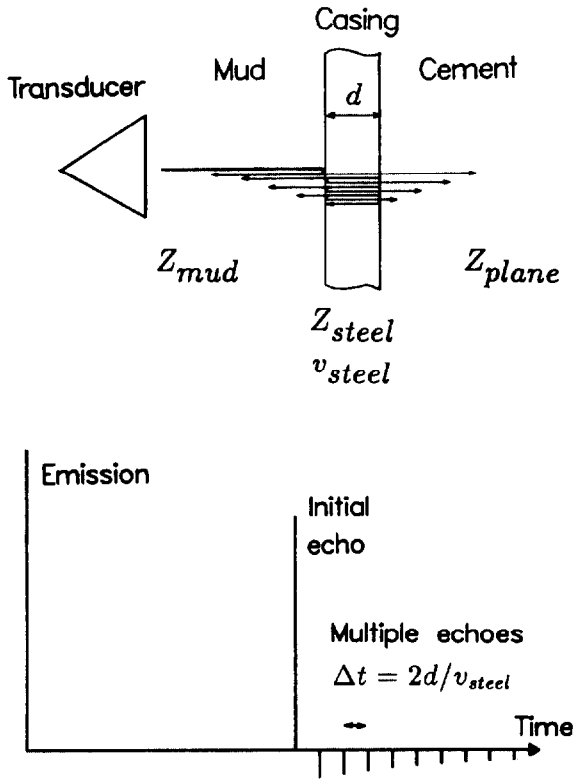
Figure 1: Ultrasonic measurement principle: planar model and impulse response
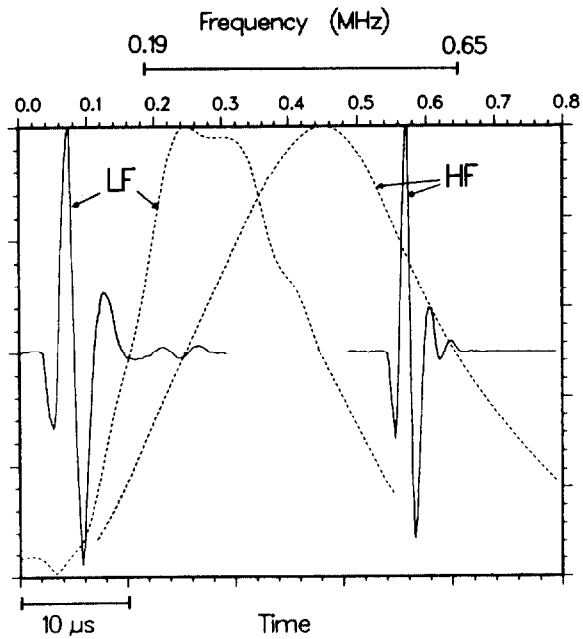
Figure 3: Time responses and bandwidths of high-frequency (HF) and low-frequency (LF) transducers
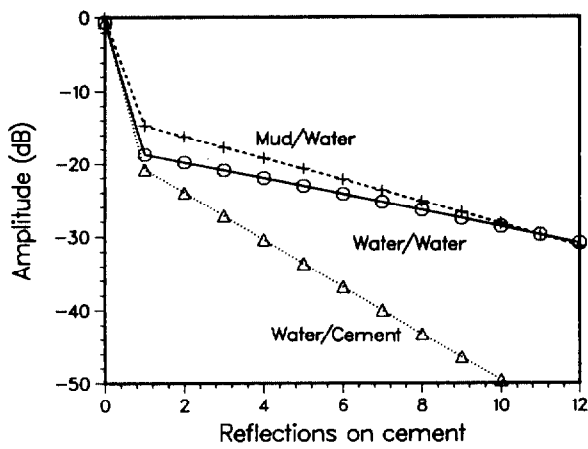
Figure 2: Influence of cement and mud on planar impulse response (dB scale). Assumed impedances: mud, 2.5 MRayl; cement 6 MRayl.
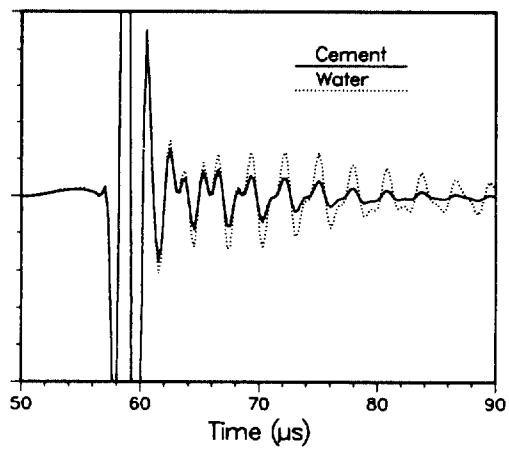
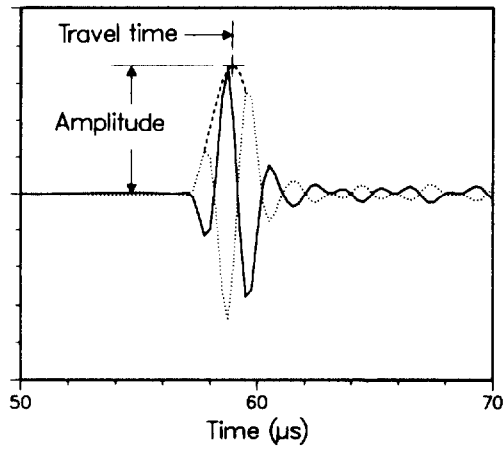Figure 4: Modeled echoes from 7-in. diameter casing with water and cement behind
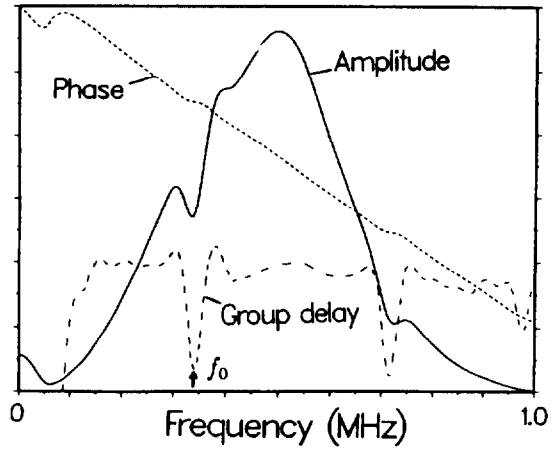
14

Figure 5: Peak location

Figure 7: Frequency spectrum of process-windowed signal from Figure 6, showing clear identification of resonances by the group-delay spectrum
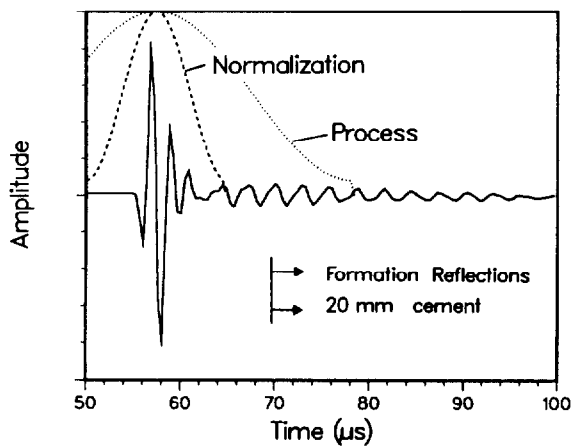
Figure 6: Typical T^3 processing windows for an 8.5-mm thick casing. The process-window half-length is 7 resonant periods; the normalization window half-length is 2.5 periods.

KK
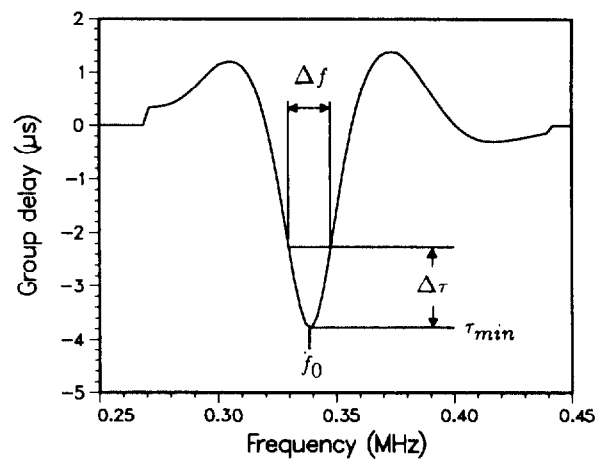
Figure 8: Group-delay characterization of the casing resonance.

15
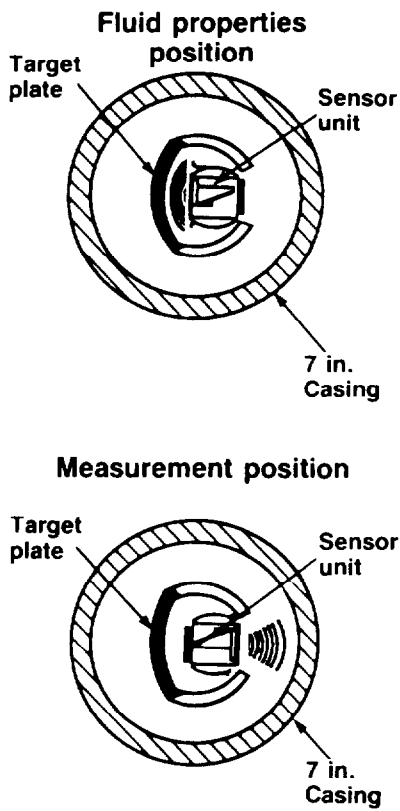
Figure 9: Downhole fluid properties measurement

Figure 11: Modeled fluid/solid effect: processed impedance versus real impedance for fluid and solid media outside a 7-in. diameter, 9-mm thick casing.

Figure 10: Correction for nonplanar geometry in a 7-in. diameter, 9-mm thick casing: T^3 fit Z_{plane} versus true fluid impedance Z_{cemf}
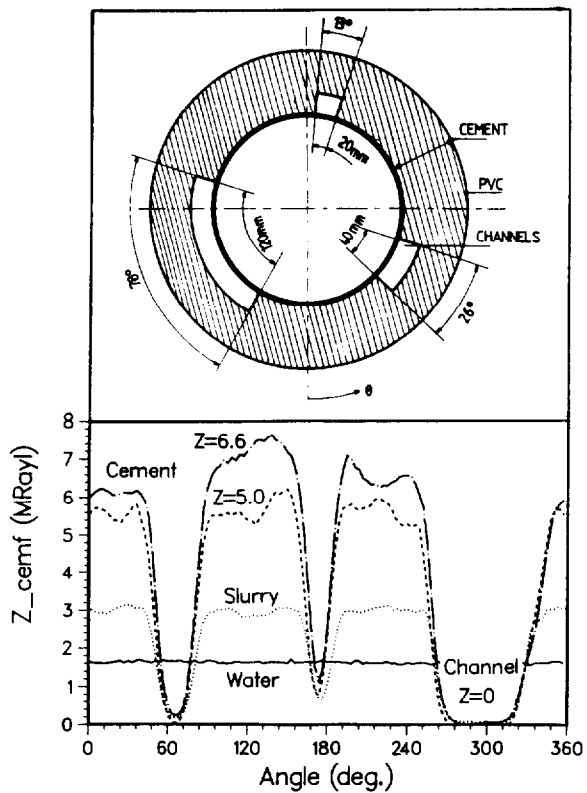
Figure 12: Laboratory measurements in a 7-in. diameter, 9-mm thick machined casing cemented with artificial channels (Z=0). Channel widths: 40 mm, 20 mm, 120 mm

16
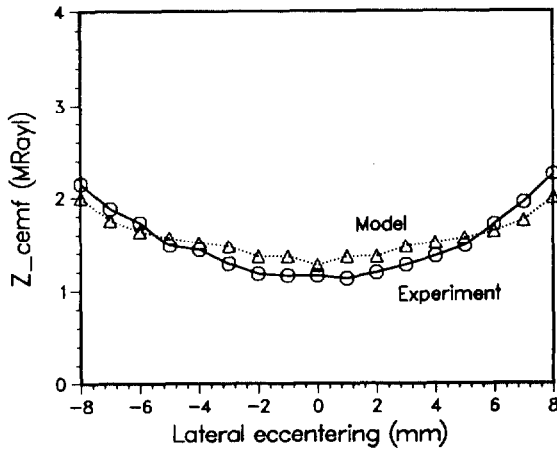
Figure 13: Effect of lateral eccentering in 7-in. diameter 8.9-mm thick casing
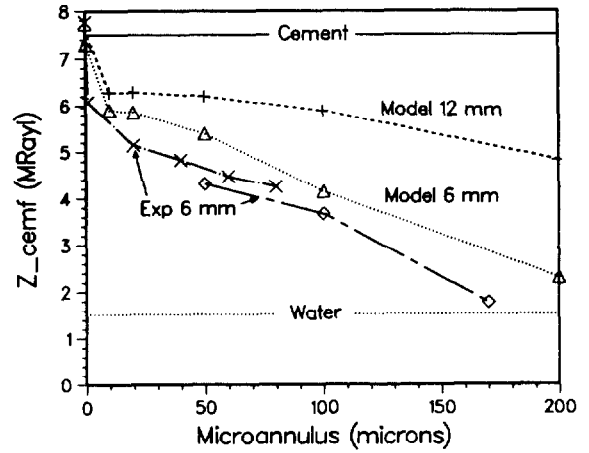
Figure 15: Experimental and theoretical effect of water microannulus outside a 7-in. diameter, 6-mm thick casing. Cement impedance = 6.3 MRayl (experiment), 6 MRayl (theory)
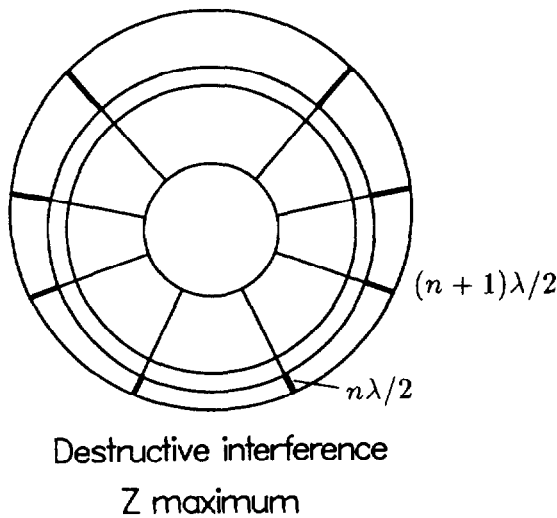

Destructive interference

Z maximum

Figure 14: Interference due to formation reflections in an eccentered casing

KK
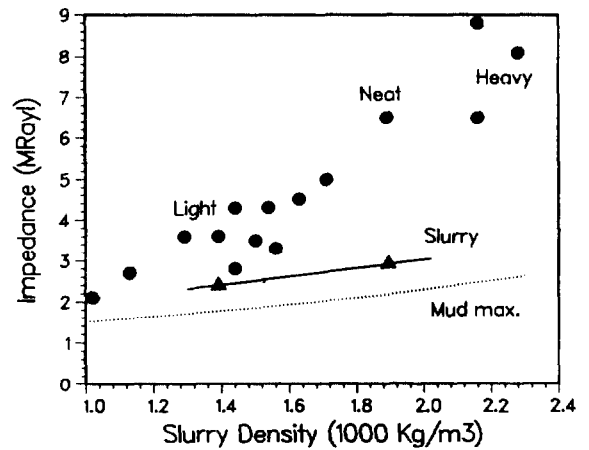
Figure 16: Acoustic impedances of cements (after 7 days or more cure at ambient conditions), slurries and mud

17

Table 2: Specifications

General	
Length	262.2 in. (6.671 m)
Weight (no sub)	377.6 lb (171.6 kg)
Diameter (no sub)	3.325 in.(85.7 mm)

Environmental	
Temperature	350° F
Pressure	20,000 psi
Min. casing O.D.	4.5 in.
Max. casing O.D.	13.325 in.
Max. deviation	No limit

Cementation	
Acoustic Impedance	
— Range	0-10 MRayl
— Resolution	0.2 MRayl
— Accuracy	± 0.5 MRayl (0–3.3 MRayl)
	± 15% (> 3.3 MRayl)
Mud density	
— Water base	<1900 kg.m^{-3} (16 lbm/gal)
— Oil base	<1400 kg.m^{-3} (11.6 lbm/gal)
Channel resolution	30 mm (1.2 in.)

Corrosion	
Inside diameter	4–14 in.
Inside radius	
— Resolution	0.05 mm (0.002 in.)
— Rel. accuracy	± 0.2 mm (0.008 in.)
Thickness	
— Range	4.5–15 mm (0.177–0.59 in.)
— Resolution	0.05 mm (0.002 in.)
— Accuracy	± 2%

Tool Combinations
Gamma ray, CBL-VDL, Cement Bond Tool,
Casing Collar Locator, Inclinometer Tool

Table 3: Logging modes

Cementation		
Sampling		Logging speed
Azimuth	Vertical	
10°	1.5 in. (38 mm)	1600 ft/hr (488 m/hr)
5°	6.0 in. (152 mm)	3200 ft/hr (975 m/hr)
5°	1.5 in. (38 mm)	800 ft/hr (244 m/hr)
5°	0.6 in. (15 mm)	300 ft/hr (91 m/hr)
Corrosion		
Sampling		Logging speed
Azimuth	Vertical	
10°	0.6 in. (15 mm)	900 ft/hr (274 m/hr)
5°	0.6 in. (15 mm)	900 ft/hr (274 m/hr)
3.3°	0.4 in. (10 mm)	900 ft/hr (274 m/hr)

Compensating device

Motor assembly

Rotating electrical connection

Centralizer

Rotating shaft

Rotating seal

Built-in electronics

Interchangeable SUB

Sensor

7.5 rps

Figure 17: USI sonde

18

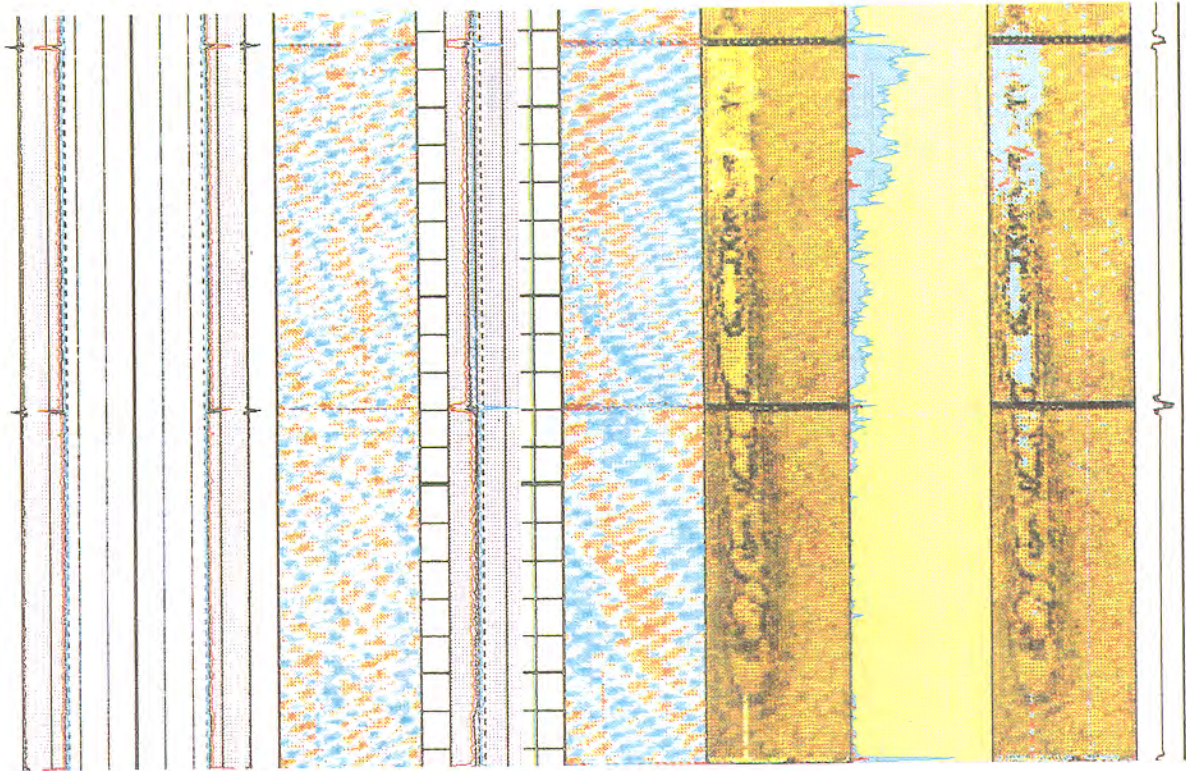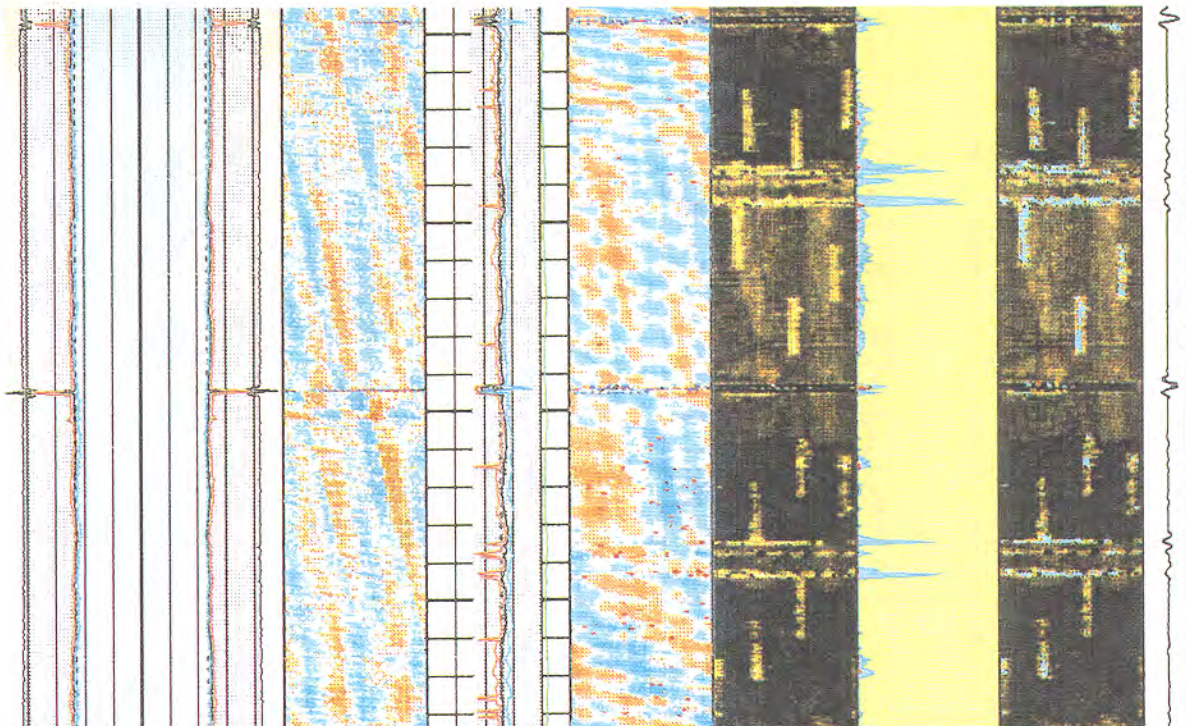| Depth Scale 1:200 M	Diagnostic flags	Amplitude - Max	Radius 3.7 2.7 (IN)	Radius 2.7 3.7 (IN)	iRadii - Ave	Cable Speed 300 500 (M/HR)	Thickness - Ave	Acoustic Imped.	Cement Map	C CL U
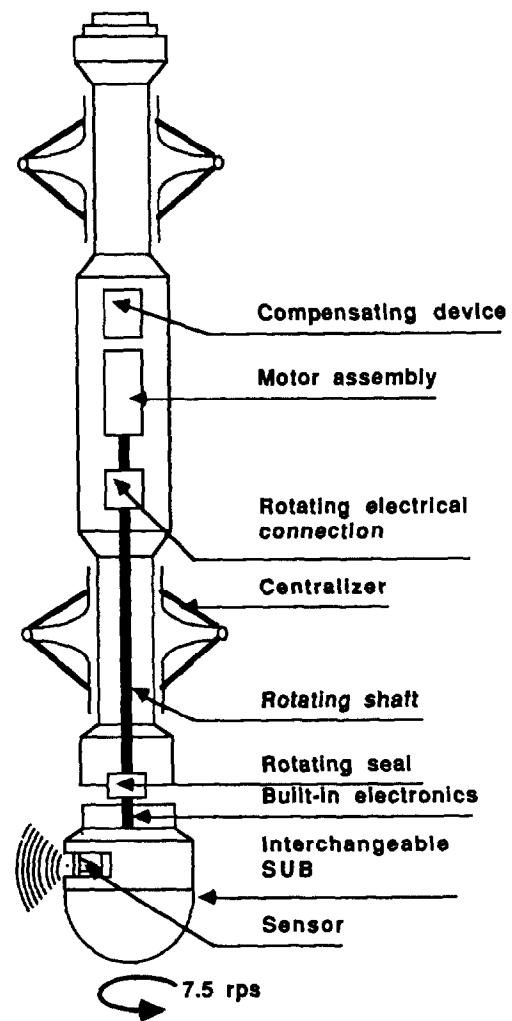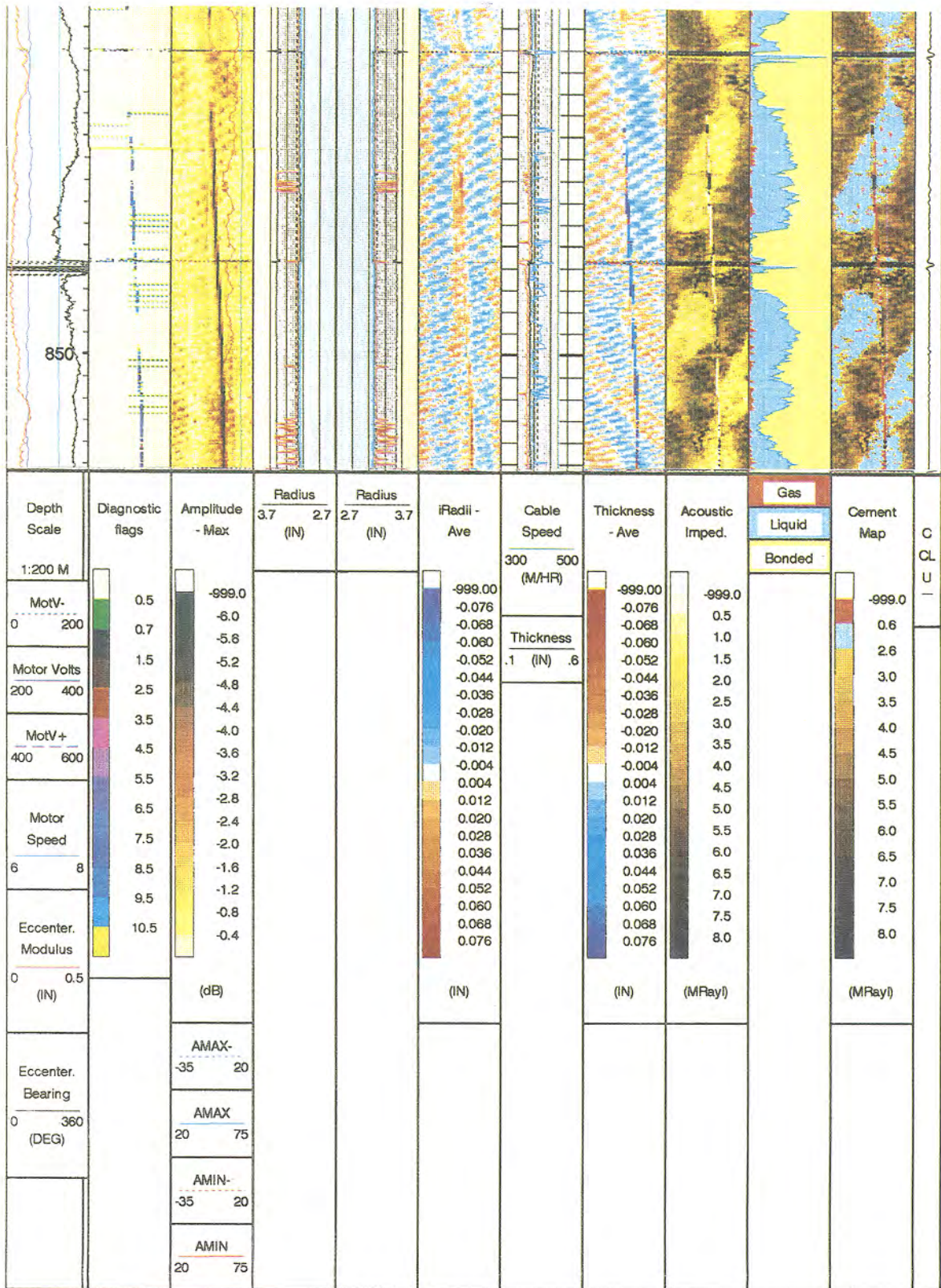
Example 1: Channeling and casing wear
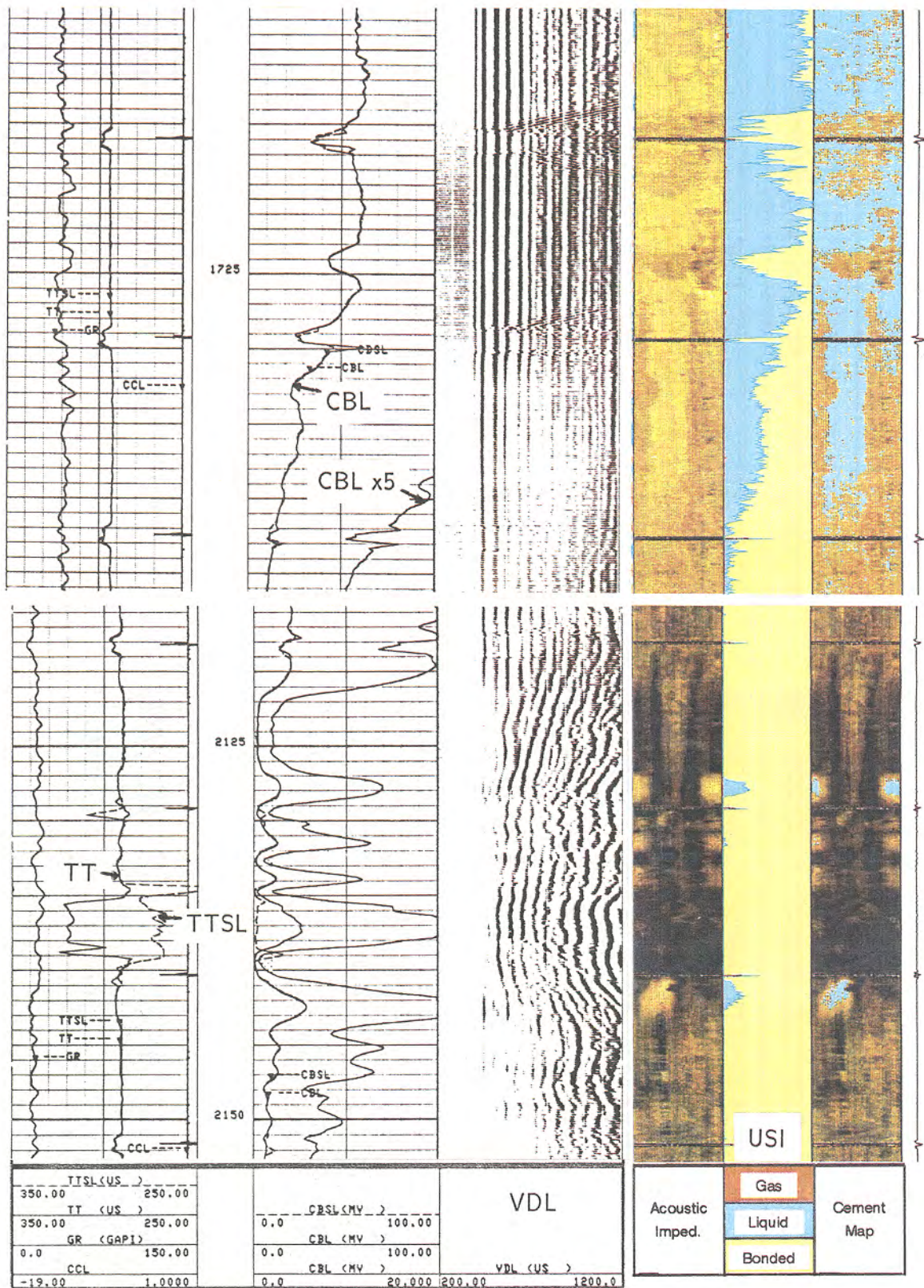
KK
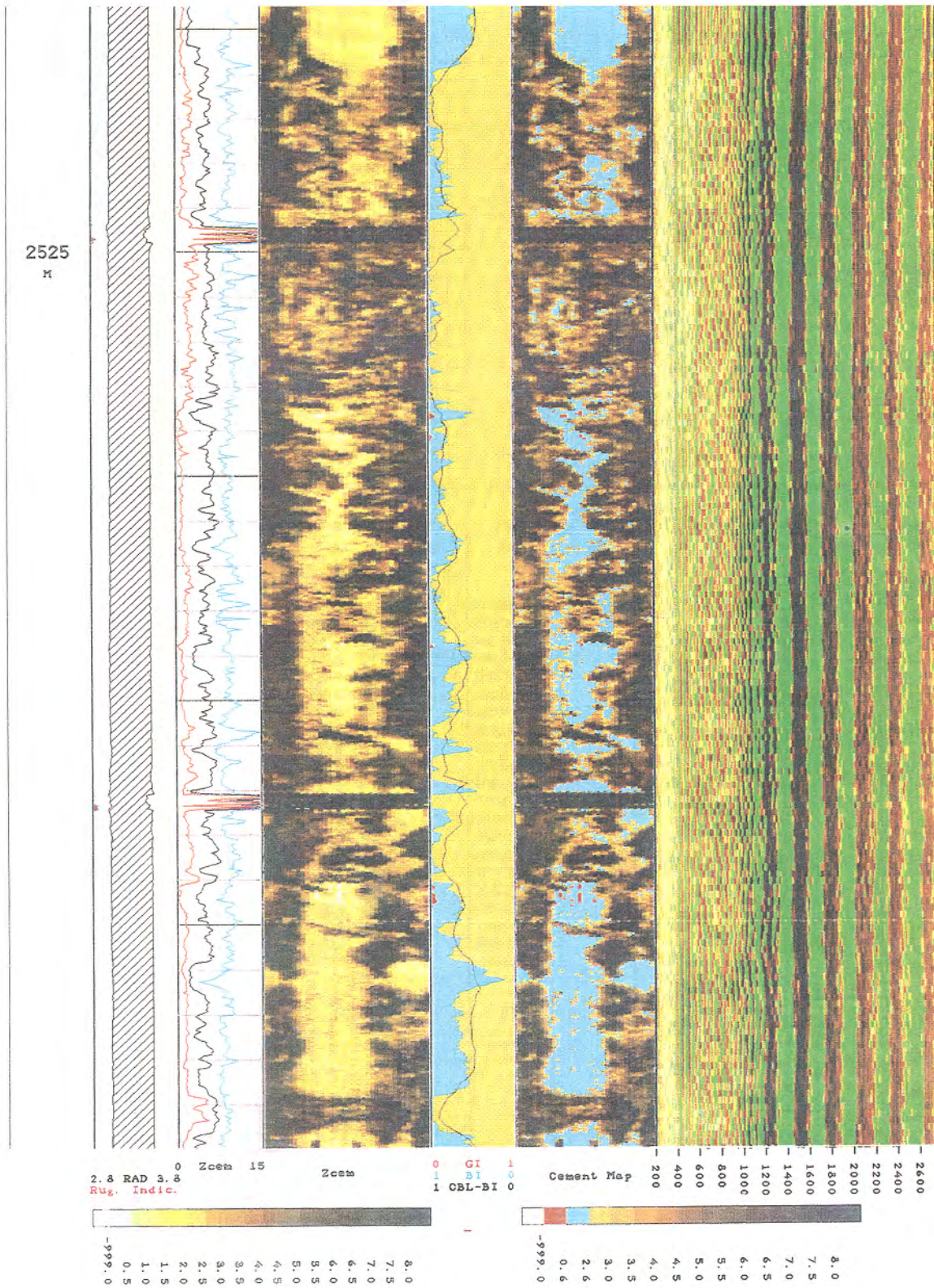
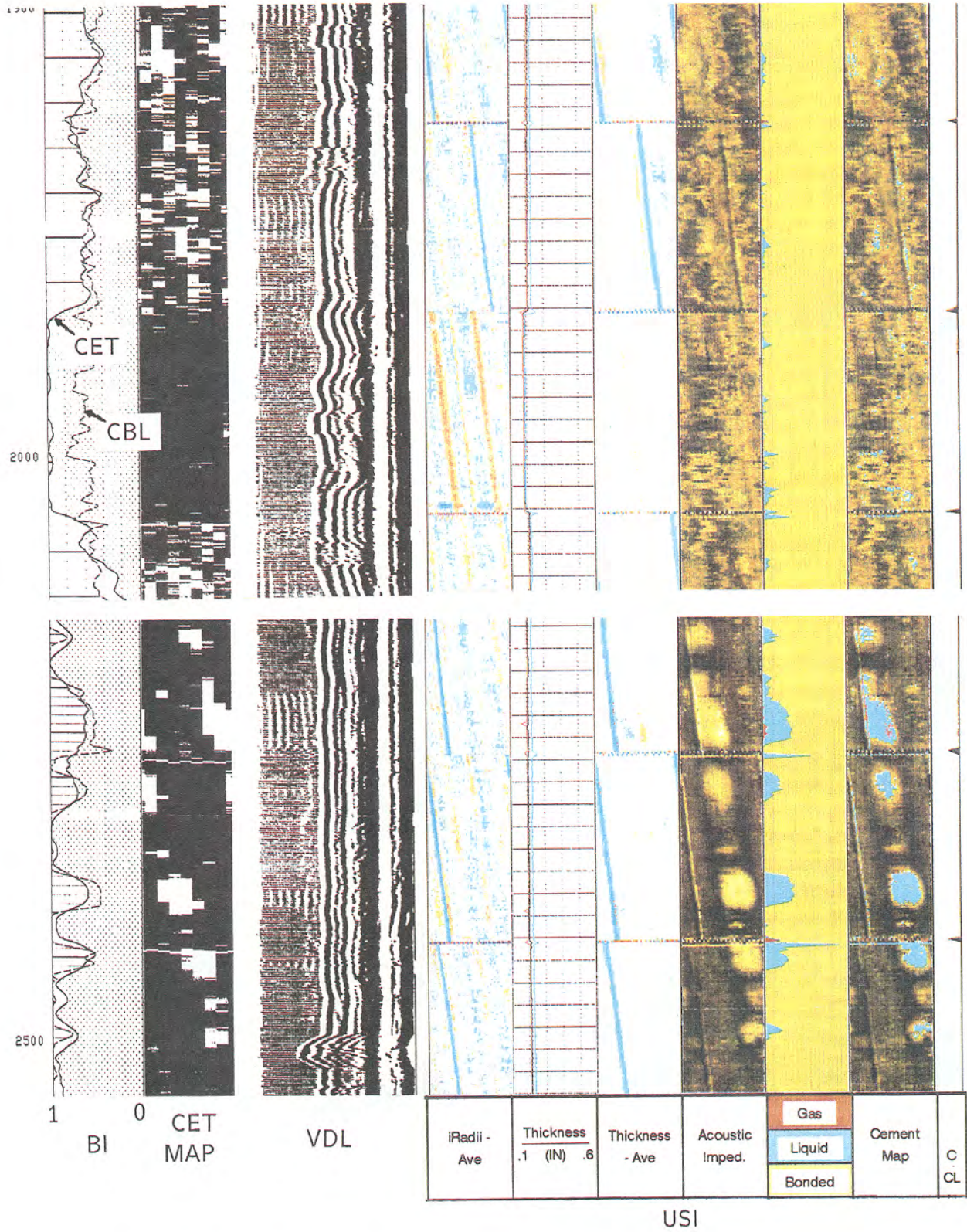**Example 2: Channeling**

Example 3: Formation reflections
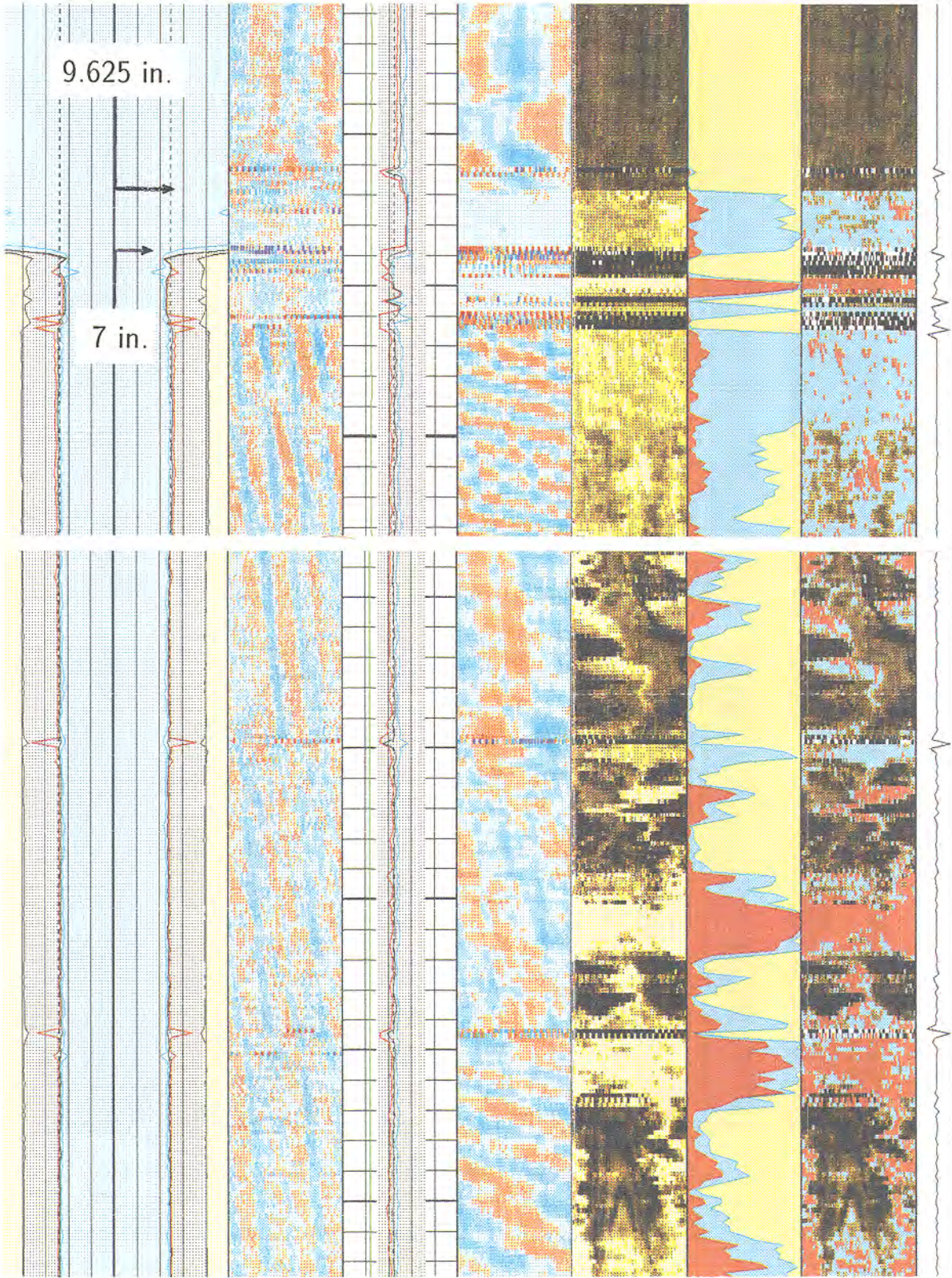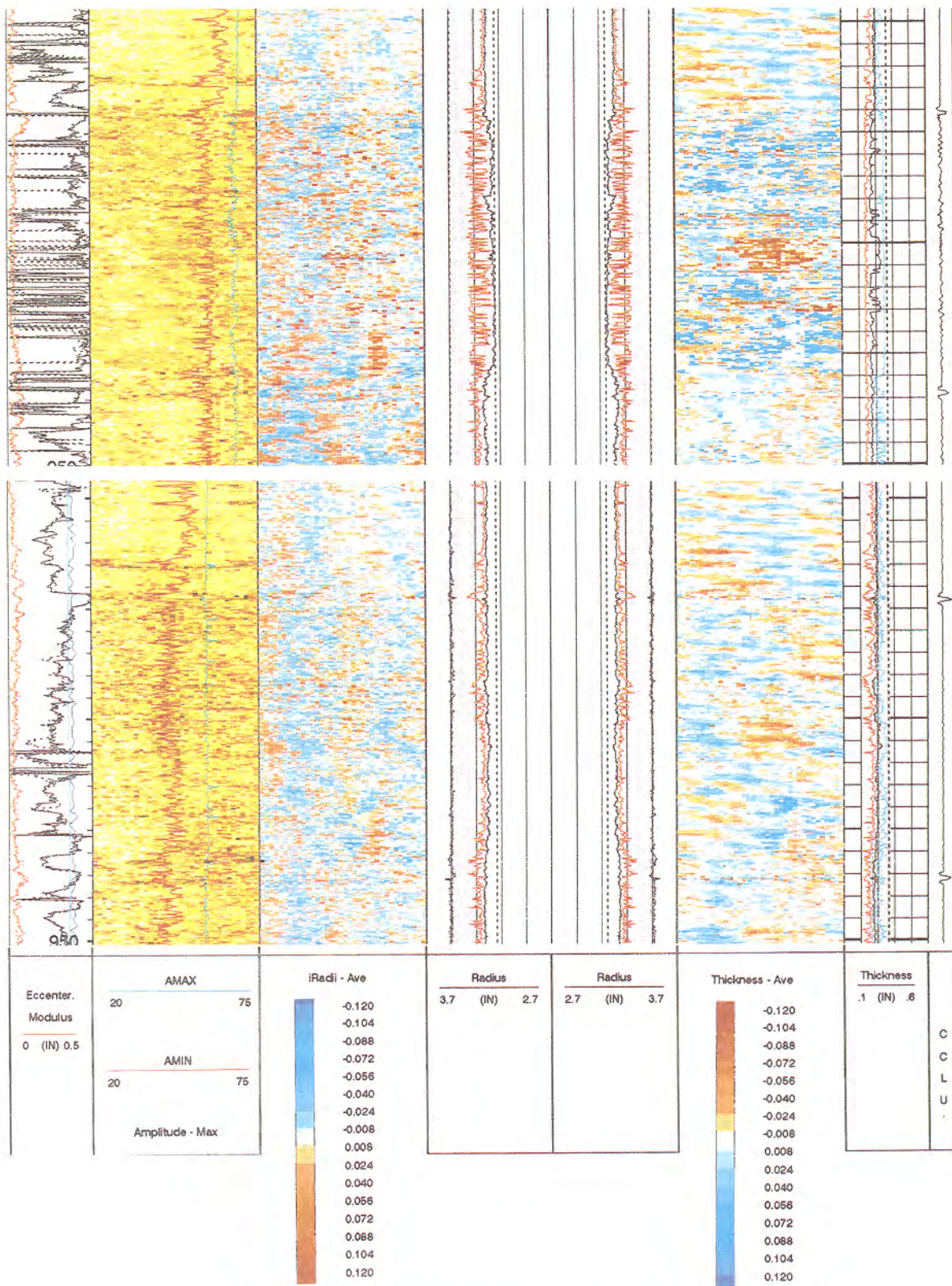

Example 4: Scratchers

KK

Example 5: Light cement, oil-base mud

Example 6: Welded casing– contaminated cement, mud channels

Example 7: Gas problem

Example 8: Generalized Corrosion

sphweb.bumc.bu.edu/otlt/MPH-Modules/BS/BS704_Confidence_Intervals/BS704_Confidence_Intervals_print.html
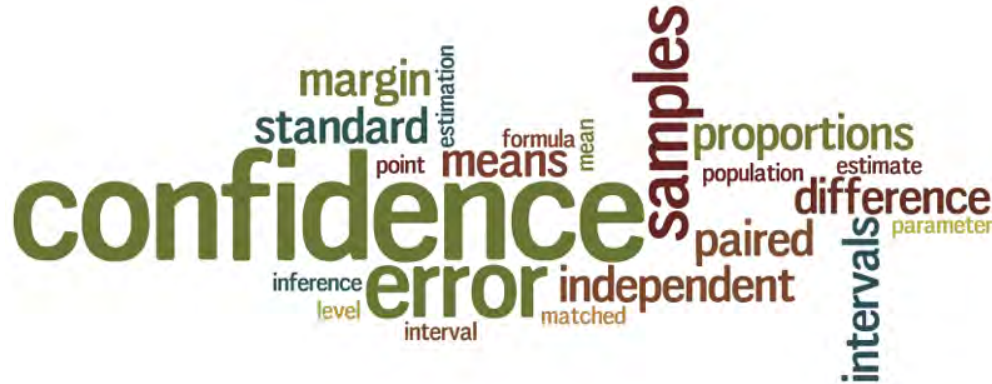
"Confidence Intervals,"
Lisa Sullivan, PhD.

Confidence Intervals

Author:

Lisa Sullivan, PhD

Professor of Biostatistics

Boston University School of Public Health

Introduction

As noted in earlier modules a key goal in applied biostatistics is to make inferences about unknown population parameters based on sample statistics. There are two broad areas of statistical inference, estimation and hypothesis testing. Estimation is the process of determining a likely value for a population parameter (e.g., the true population mean or population proportion) based on a random sample. In practice, we select a sample from the target population and use sample statistics (e.g., the sample mean or sample proportion) as estimates of the unknown parameter. The sample should be representative of the population, with participants selected at random from the population. In generating estimates, it is also important to quantify the precision of estimates from different samples.

Learning Objectives

After completing this module, the student will be able to:

1. Define point estimate, standard error, confidence level and margin of error
2. Compare and contrast standard error and margin of error
3. Compute and interpret confidence intervals for means and proportions
4. Differentiate independent and matched or paired samples
5. Compute confidence intervals for the difference in means and proportions in independent samples and for the mean difference in paired samples
6. Identify the appropriate confidence interval formula based on type of outcome variable and number of samples

Boston University School of Public Health

Parameter Estimation

There are a number of population parameters of potential interest when one is estimating health outcomes (or "endpoints"). Many of the outcomes we are interested in estimating are either continuous or dichotomous variables, although there are other types which are discussed in a later module. The parameters to be estimated depend not only on whether the endpoint is continuous or dichotomous, but also on the number of groups being studied. Moreover, when two groups are being compared, it is important to establish whether the groups are independent (e.g., men versus women) or dependent (i.e., matched or paired, such as a before and after comparison).   The table below summarizes parameters that may be important to estimate in health-related studies.

	Parameters Being Estimated	
	Continuous Variable	Dichotomous Variable
One Sample	mean	proportion or rate, e.g., prevalence, cumulative incidence, incidence rate
Two Independent Samples	difference in means	difference in proportions or rates, e.g., risk difference, rate difference, risk ratio, odds ratio, attributable proportion
Two Dependent, Matched Samples	mean difference	

Confidence Intervals

There are two types of estimates for each population parameter: the point estimate and confidence interval (CI) estimate. For both continuous variables (e.g., population mean) and dichotomous variables (e.g., population proportion) one first computes the point estimate from a sample. Recall that sample means and sample proportions are unbiased estimates of the corresponding population parameters.

For both continuous and dichotomous variables, the **confidence interval estimate (CI)** is a range of likely values for the population parameter based on:

- the point estimate, e.g., the sample mean
- the investigator's desired level of confidence (most commonly 95%, but any level between 0-100% can be selected)
- and the sampling variability or the standard error of the point estimate.

Strictly speaking a 95% confidence interval means that if we were to take 100 different samples and compute a 95% confidence interval for each sample, then approximately 95 of the 100 confidence intervals will contain the true mean value (μ). In practice, however, we select one random sample and generate one confidence interval, which may or may not contain the true mean. The observed interval may over- or underestimate μ. Consequently, the 95% CI is the likely range of the true, unknown parameter. The confidence interval does not reflect the variability in the unknown parameter. Rather, it reflects the amount of random error in the sample and provides a range of values that are likely to include the unknown parameter. Another way of thinking about a confidence interval is that it is the range of likely values of the parameter (defined as the point estimate $\pm$ margin of error) with a specified level of confidence (which is similar to a probability).

CalAdvocates - 634

Suppose we want to generate a 95% confidence interval estimate for an unknown population mean. This means that there is a 95% probability that the confidence interval will contain the true population mean. Thus, P([sample mean] - margin of error < μ < [sample mean] + margin of error) = 0.95.

The Central Limit Theorem introduced in the module on Probability stated that, for large samples, the distribution of the sample means is approximately normally distributed with a mean:

$$\mu_{\overline{X}} = \mu$$

and a standard deviation (also called the standard error):

$$\sigma_{\overline{x}} = \sigma / \sqrt{n}$$

For the standard normal distribution, P(-1.96 < Z < 1.96) = 0.95, i.e., there is a 95% probability that a standard normal variable, Z, will fall between -1.96 and 1.96. The Central Limit Theorem states that for large samples:

$$z = \frac{\overline{X} - \mu_{\overline{x}}}{\sigma_{\overline{x}}} = \frac{\overline{X} - \mu}{\sigma / \sqrt{n}}$$

By substituting the expression on the right side of the equation:

$$P\left(-1.96 < \frac{\overline{X} - \mu}{\sigma / \sqrt{n}} < 1.96\right) = 0.95$$

Using algebra, we can rework this inequality such that the mean (μ) is the middle term, as shown below.

$$P\left(-1.96\,\sigma / \sqrt{n} < \mu < \overline{X} + 1.96\,\sigma / \sqrt{n}\right) = 0.95$$

then

$$P\left(-1.96\,\sigma / \sqrt{n} < \mu < \overline{X} + 1.96\,\sigma / \sqrt{n}\right) = 0.95$$

and finally

$$P\left(-1.96\,\sigma / \sqrt{n} < \mu < \overline{X} + 1.96\,\sigma / \sqrt{n}\right) = 0.95$$

This last expression, then, provides the 95% confidence interval for the population mean, and this can also be expressed as:

$$\overline{X} \pm 1.96\,\sigma / \sqrt{n}$$

Thus, the margin of error is 1.96 times the standard error (the standard deviation of the point estimate from the sample), and 1.96 reflects the fact that a 95% confidence level was selected. So, the general form of a confidence interval is:

point estimate ± Z SE (point estimate)

where Z is the value from the standard normal distribution for the selected confidence level (e.g., for a 95% confidence level, Z=1.96).

In practice, we often do not know the value of the population standard deviation (**σ**). However, if the sample size is large (n ≥ 30), then the sample standard deviations can be used to estimate the population standard deviation.